



**HAL**  
open science

## Structural and mechanistic insights into the function of Leishmania ribosome lacking a single pseudouridine modification

K. Shanmugha Rajan, Saurav Aryal, Disha-Gajanan Hiregange, Anat Bashan,  
Hava Madmoni, Mika Olami, Tirza Doniger, Smadar Cohen-Chalamish,  
Pascal Pescher, Masato Taoka, et al.

### ► To cite this version:

K. Shanmugha Rajan, Saurav Aryal, Disha-Gajanan Hiregange, Anat Bashan, Hava Madmoni, et al.. Structural and mechanistic insights into the function of Leishmania ribosome lacking a single pseudouridine modification. Cell Reports, 2024, 43 (5), pp.114203. 10.1016/j.celrep.2024.114203 . pasteur-04607773

**HAL Id: pasteur-04607773**

**<https://pasteur.hal.science/pasteur-04607773>**

Submitted on 11 Jun 2024

**HAL** is a multi-disciplinary open access archive for the deposit and dissemination of scientific research documents, whether they are published or not. The documents may come from teaching and research institutions in France or abroad, or from public or private research centers.

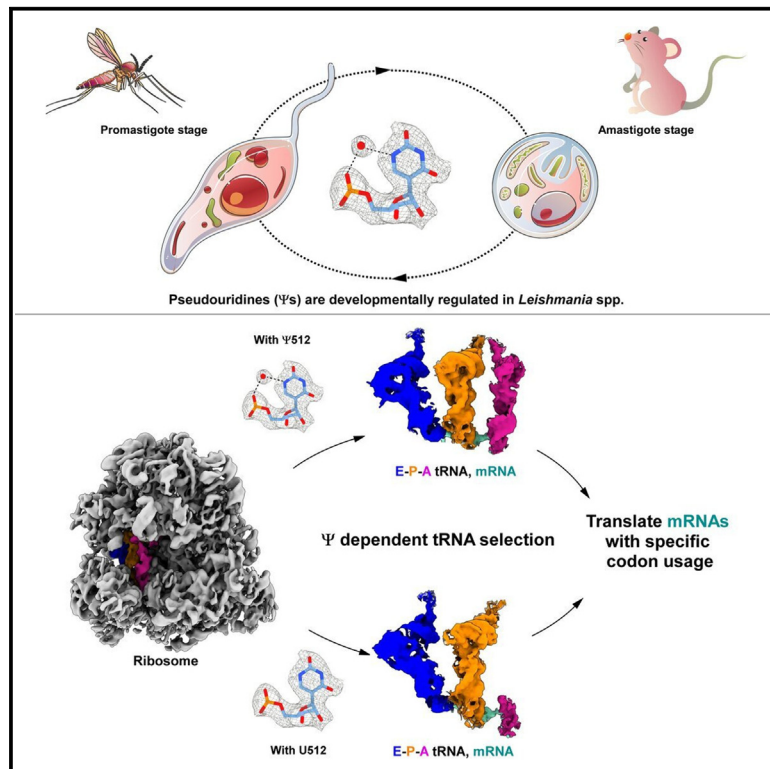
L'archive ouverte pluridisciplinaire **HAL**, est destinée au dépôt et à la diffusion de documents scientifiques de niveau recherche, publiés ou non, émanant des établissements d'enseignement et de recherche français ou étrangers, des laboratoires publics ou privés.



Distributed under a Creative Commons Attribution - NonCommercial 4.0 International License

# Structural and mechanistic insights into the function of *Leishmania* ribosome lacking a single pseudouridine modification

## Graphical abstract



## Authors

K. Shanmugha Rajan, Saurav Aryal, Disha-Gajanan Hiregange, ..., Gerald F. Späth, Ada Yonath, Shulamit Michaeli

## Correspondence

shulamit.michaeli@biu.ac.il

## In brief

Rajan et al. demonstrate the significance of a single rRNA modification for the structure and the function of ribosomes, thus affecting the translation of a subset of mRNAs. The changes in ribosome structure affect tRNA selectivity, resulting in codon bias.

## Highlights

- $\Psi$  modification on rRNA is developmentally regulated in *Leishmania* parasite
- Ablation of a single  $\Psi$  modification affects translation of a subset of mRNAs
- $\Psi$  modification on rRNA affects its structure and its interactions with specific tRNAs



## Article

# Structural and mechanistic insights into the function of *Leishmania* ribosome lacking a single pseudouridine modification

K. Shanmugha Rajan,<sup>1,2</sup> Saurav Aryal,<sup>2</sup> Disha-Gajanan Hiregange,<sup>1</sup> Anat Bashan,<sup>1</sup> Hava Madmoni,<sup>2</sup> Mika Olami,<sup>2</sup> Tirza Doniger,<sup>2</sup> Smadar Cohen-Chalamish,<sup>2</sup> Pascal Pescher,<sup>3</sup> Masato Taoka,<sup>4</sup> Yuko Nobe,<sup>4</sup> Aliza Fedorenko,<sup>1</sup> Tanaya Bose,<sup>1</sup> Ella Zimmermann,<sup>1</sup> Eric Prina,<sup>3</sup> Noa Aharon-Hefetz,<sup>5</sup> Yitzhak Pilpel,<sup>5</sup> Toshiaki Isobe,<sup>4</sup> Ron Unger,<sup>2</sup> Gerald F. Späth,<sup>3</sup> Ada Yonath,<sup>1</sup> and Shulamit Michaeli<sup>2,6,\*</sup>

<sup>1</sup>Department of Chemical and Structural Biology, The Weizmann Institute of Science, Rehovot 76100001, Israel

<sup>2</sup>The Mina and Everard Goodman Faculty of Life Sciences and Advanced and Nanotechnology Institute, Bar-Ilan University, Ramat-Gan 52900, Israel

<sup>3</sup>Institut Pasteur, Université Paris Cité, INSERM U1201, Unité de Parasitologie moléculaire et Signalisation, Paris, France

<sup>4</sup>Department of Chemistry, Graduate School of Science, Tokyo Metropolitan University, Minami-osawa 1-1, Hachioji-shi, Tokyo 192-0397, Japan

<sup>5</sup>Department of Molecular Genetics, Weizmann Institute of Science, Rehovot, Israel

<sup>6</sup>Lead contact

\*Correspondence: [shulamit.michaeli@biu.ac.il](mailto:shulamit.michaeli@biu.ac.il)

<https://doi.org/10.1016/j.celrep.2024.114203>

## SUMMARY

*Leishmania* is the causative agent of cutaneous and visceral diseases affecting millions of individuals worldwide. Pseudouridine ( $\Psi$ ), the most abundant modification on rRNA, changes during the parasite life cycle. Alterations in the level of a specific  $\Psi$  in helix 69 (H69) affected ribosome function. To decipher the molecular mechanism of this phenotype, we determine the structure of ribosomes lacking the single  $\Psi$  and its parental strain at  $\sim 2.4\text{--}3\text{ \AA}$  resolution using cryo-EM. Our findings demonstrate the significance of a single  $\Psi$  on H69 to its structure and the importance for its interactions with helix 44 and specific tRNAs. Our study suggests that rRNA modification affects translation of mRNAs carrying codon bias due to selective accommodation of tRNAs by the ribosome. Based on the high-resolution structures, we propose a mechanism explaining how the ribosome selects specific tRNAs.

## INTRODUCTION

The protozoan parasite *Leishmania* causes leishmaniasis, which represent a group of vector-borne, neglected tropical diseases affecting more than 12 million people in  $\sim 99$  countries. Visceral leishmaniasis, also known as Kala Azar, is caused by *Leishmania donovani* (*L. donovani*) and may lead to death in less-developed countries in the absence of accessible treatment.<sup>1</sup> Cutaneous leishmaniasis is caused by species including *L. major* and *L. amazonensis*.<sup>1</sup> Leishmaniasis control is limited because of the absence of vaccines, and although several drugs exist, most of them are toxic or rather ineffective due to the emergence of drug resistance.<sup>2</sup> The *Leishmania* parasite has a digenetic life cycle infecting two hosts: motile extracellular promastigotes replicate in the midgut of the sand fly insect vector, while immotile intracellular amastigotes proliferate inside phagolysosomes of mammalian macrophages.<sup>3</sup>

Regulation of gene expression in *Leishmania* is unique because these parasites, including the related trypanosomes, lack canonical core promoter elements for protein-coding genes, and transcription is polycistronic and constitutive.<sup>4</sup> Gene regulation in these organisms is mainly post-transcrip-

tional at the level of mRNA stability and translation. Hence, it is mediated by hundreds of RNA-binding proteins<sup>4,5</sup> and by the recently described antisense regulators.<sup>6</sup>

rRNA modification was demonstrated to control gene expression during development and disease.<sup>7</sup> The most abundant modifications on rRNA are pseudouridine ( $\Psi$ ) and 2'-O-methylation (Nm),<sup>8</sup> which are guided by small nucleolar RNA (snoRNA).<sup>9-11</sup> The  $\Psi$  on rRNA is guided by H/ACA snoRNAs and depends on the formation of the pseudouridylation pocket between the target and non-consecutive interaction domain of the snoRNA.<sup>10,11</sup>  $\Psi$  increases the potential for the formation of an extra hydrogen bond between bases, compared with uridine, which contributes to structural stability and increased stacking interactions of the RNA.<sup>12,13</sup>  $\Psi$  can either strengthen or weaken RNA-protein interactions.<sup>14-16</sup>

The influence of  $\Psi$ s on human rRNA differ among different tissues and organs, as well as in cancer cells.<sup>17,18</sup> Impaired rRNA pseudouridylation in dyskeratosis congenita patient cells affects the translation of a subset of mRNAs.<sup>19</sup> In yeast, global translation and fidelity are impaired when more than a single  $\Psi$  on the decoding center, helix 69 (H69), and peptidyl transferase center (PTC) are altered.<sup>20-22</sup> However, no significant effect



was observed following changes of a single modification.<sup>20–22</sup> Recently, the cryo-EM structure of a  $\Psi$ -free yeast ribosome showed abnormal inter-subunit movements that most likely are responsible for defects in translation.<sup>23</sup> We previously demonstrated that in trypanosomes,  $\Psi$  is developmentally regulated between the two life stages of the parasite on rRNA, snRNAs, mRNAs, and other non-coding RNAs, and that hypermodification contributes to temperature adaptation during cycling between the insect and the mammalian hosts.<sup>14–16</sup>

X-ray crystal structure of ribosome revealed that the loop of H69 contacts the minor groove of A-site tRNA D-stem junction, and the stem structure of H69 contacts the minor groove of the P-site tRNA D stem. In addition, the loop of H69 also contacts the minor groove of helix 44 of small subunit (SSU) rRNA adjacent to the decoding site forming the intersubunit bridge B2a.<sup>24</sup> Previous studies from our group suggested that H69 might act like a molecular “crane” in moving the tRNA from the A- to the P-site in the ribosome.<sup>25,26</sup> Functional analysis using deletion strains of *E. coli* H69 ( $\Delta$ h69) suggested that the large subunit (LSU) is unable to associate with the SSU in the absence of tRNA, providing direct evidence that disruption in B2a bridge is sufficient to prevent subunit association.<sup>27</sup> Studies of *E. coli* H69 mutants suggested that A1913 in the H69 loop forms necessary contacts for efficient accommodation of a subset of natural tRNA species.<sup>28</sup>

Different from most eukaryotic ribosomes, the LSU rRNA of the ribosomes of *Leishmania* is processed into two large (LSU $\alpha$  and  $\beta$ ) and four small fragments (srRNA1, 2, 4, and 6).<sup>29–31</sup> In this study, we determined the landscape of  $\Psi$ s on rRNA from *L. donovani*, *L. amazonensis*, and *L. major* in promastigote and amastigote stages. A single  $\Psi$  modification ( $\Psi$ 512) located in H69 was found to be differentially regulated in the two life stages of all three *Leishmania* species. To understand how a change in single  $\Psi$  can affect ribosome structure and function, high-resolution cryoelectron microscopy (cryo-EM) structures of *L. major* ribosomes of the parental strain (PS) and LM32Cs3H1 single knockout (sKO) were determined. The cryo-EM structure of the sKO ribosome compared with PS showed distinct changes in the architecture of H69 and enabled us to propose structural insights into the mechanism by which *Leishmania* selects specific tRNA to accommodate specific codon usage.

## RESULTS

### Identification and quantification of $\Psi$ s in different *Leishmania* species that demonstrate species- and stage-specific modifications

Based on the finding that  $\Psi$  and Nm are developmentally regulated in the extracellular trypanosome parasites,<sup>14–16,32,33</sup> we assessed such property in *Leishmania*, which is an intracellular parasite. Our previous studies in *L. major* identified 81 H/ACA snoRNA predicted to guide  $\Psi$ s on rRNA.<sup>34</sup> In this study, we identified the H/ACA snoRNA population from three *Leishmania* species (*L. donovani*, *L. major*, and *L. amazonensis*) that potentially guide 61, 64, and 67  $\Psi$ s, respectively, on the rRNA (Table S1). To verify the presence of the predicted  $\Psi$ s, we performed two genome-wide mapping studies by  $\Psi$ -seq<sup>14–16</sup> and HydraPsiSeq<sup>35</sup> on rRNA from promastigotes and amastigotes in three species (*L. donovani*, *L. major*, and *L. amazonensis*).

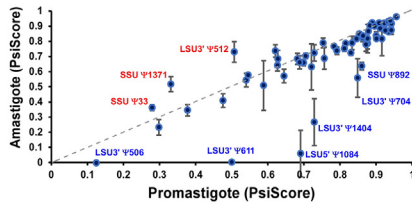
The amastigotes used in this study were derived from infected animals (hamster and mice), thus the parasites were exposed to the natural environment during infection. The results demonstrate that both methods identified identical positions of  $\Psi$ s (Figures S1 and S2; Table S1). Two species-specific  $\Psi$ s were found in *L. donovani* and in *L. amazonensis* (Table S1). HydraPsiSeq was used to identify any differences in stoichiometry between the species and the life stages. In *L. donovani*, three sites were hypermodified, and six sites were hypomodified in amastigotes, compared with promastigotes (Figure 1A). In *L. amazonensis*, three sites were hypermodified and only three sites were hypomodified in amastigotes compared with promastigotes (Figures 1A; Table S1). Whereas in *L. major*, ten sites were hypermodified and one site was hypomodified (Figures 1A; Table S1). Superimposing the hyper- and hypomodified sites on the 3D structure of the *Leishmania* ribosome showed that these differentially regulated sites are not located in or around functional domains, except one site,  $\Psi$ 512 in H69, which is hypermodified in *L. donovani* and *L. major* but hypomodified in *L. amazonensis* (Figure 1B).

### Overexpression of LM32Cs3H1 snoRNA guiding $\Psi$ 512 on H69 affects growth and translation

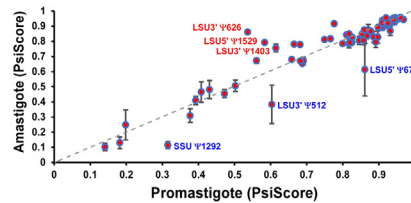
The  $\Psi$ 512 present in H69 was found to be differentially regulated between promastigotes and amastigotes of all three *Leishmania* species (Figures 1A and 1B). A higher level (~37%–39%) of  $\Psi$ 512 was identified in *L. donovani* and *L. major* amastigote rRNA, and a lower level (~23%) in *L. amazonensis* amastigote rRNA. Compared with other  $\Psi$ s located in H69, this property is unique to  $\Psi$ 512 (Figure 2A). To better understand the impact of  $\Psi$ 512 on ribosome function, the wild-type snoRNA LM32Cs3H1, and a version mutated in the pseudouridylation pocket (Figure 2Bi) that was expected to perturb its guiding capability were overexpressed in *L. major*. Overexpression was achieved by cloning the snoRNA along with its flanking sequences in the episomal pX vector.<sup>36</sup> Northern blot analysis showed that the level of expression was increased by 12- and 8-fold for wild-type and mutated LM32Cs3H1 versions, respectively, while no change was observed in the mock control, transfected with the empty pX vector (Figure 2Bii). The overexpression of wild-type snoRNA, but not its mutant derivative or empty vector, led to a 23% increase in the level of  $\Psi$  based on HydraPsiSeq mapping (Figure 2Biii). Overexpression of the wild-type snoRNA compromised the growth of the transgenic promastigote parasites, but no growth effect was observed in the control cells expressing the mutated snoRNA or the pX empty vector (Figure 2C). The parasites expressing the wild-type snoRNA, mutated snoRNA or the empty pX vector were used to infect macrophages derived *in vitro* from THP1 monocytes (Figure 2Di and ii). We monitored infection using parasites expressing mCherry fluorescent protein; to validate that both parasites expressing the wild-type snoRNA and the empty vector expressed equal amount of mCherry protein, its level was measured by western blot analysis (Figure 2Dii). Overexpression of the wild-type snoRNA also compromised the infection in macrophages, but overexpression of mutated-snoRNA partially recovered infection, possibly because the snoRNA may have additional regulatory functions (Figure 2Dii).

A

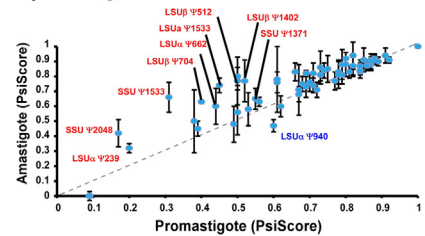
i) *L. donovani*



ii) *L. amazonensis*

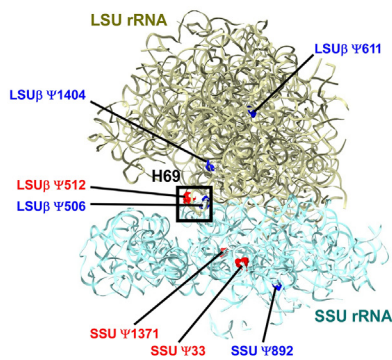


iii) *L. major*

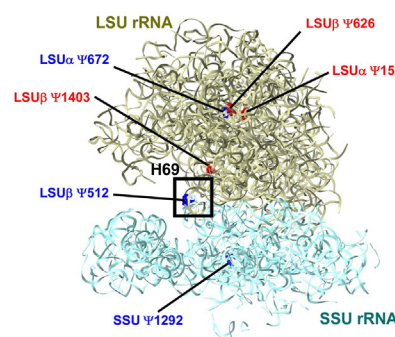


B

i) *L. donovani*



ii) *L. amazonensis*



iii) *L. major*

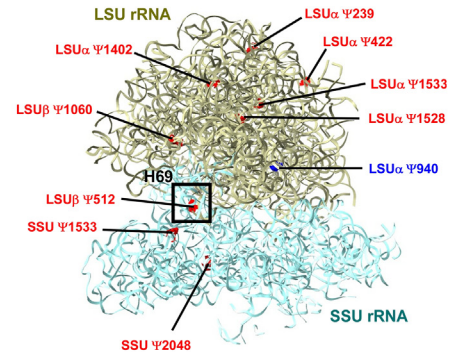


**Figure 1. Ψs on *Leishmania* rRNA are developmentally regulated**

(A) HydraPsiSeq analysis of RNA derived from amastigote and promastigote forms. (i) PsiScore (fraction pseudouridylated) is presented across the *L. donovani* rRNA molecules, and the identity of Ψ site is indicated. Data are presented as mean ± SEM. At least three biological replicates ( $n = 3$ ) were used for the quantification. (ii) As in (i) for *L. amazonensis*. (iii) As in (i) for *L. major*.

(B) Localization of variable Ψ sites on the *Leishmania* ribosome. (i) Differentially regulated Ψ sites in *L. donovani* amastigote and promastigote rRNA are shown. Ψ sites increased in amastigotes (compared with promastigotes) are depicted in red, and those decreased are shown in blue. (ii) As in (i) for *L. amazonensis*. (iii) As in (i) for *L. major*.

To examine if the promastigote growth retardation results from an effect on protein synthesis, global translation was analyzed using a fluorescent assay (see [Star methods](#)). A slight non-significant decrease in methionine incorporation was observed upon overexpression of the wild-type snoRNA (Figure 2E). Next, we examined changes in the proteome using dimethyl labeling. This method is quantitative, does not require the *in vivo* incorporation of the isotope, and is quick and efficient.<sup>37</sup> Using this method, we quantified 2,640 proteins. Based on three biological replicates, 28 proteins were significantly altered by 1.4-fold ( $p < 0.05$ ) upon wild-type snoRNA overexpression (Figure 2Fi). Note that the level of three proteins was also similarly altered upon overexpression of the defective mutant snoRNA (Figure 2Fii), suggesting that not all the changes in protein abundance in the snoRNA-overexpressing cells result from the direct effect of the altered ribosome on translation (see [discussion](#)).

### sKO by CRISPR-Cas9 of LM32Cs3H1 and LM14Cs1H3 affects translation

Both LM32Cs3H1 and LM14Cs1H3 snoRNAs guide Ψ512 and Ψ506, respectively, on H69 (Figure 3Ai) and are encoded by solitary genes.<sup>34</sup> To perform KO of the snoRNA gene, *L. major* promastigotes constitutively expressing spCas9 from the pTB007

plasmid were used.<sup>38</sup> Two guide RNAs were used to target the spCas9 to the flanking sequence of the snoRNA. To select for the KO cells, a homologous DNA repair (HDR) template carrying the puromycin resistance gene flanked by 30 nucleotides that are homologous to sequences upstream and downstream of the cleavage sites was used. The HDR PCR product was transfected along with the *in-vitro*-synthesized gRNAs, and transfected parasites were selected for puromycin resistance. Among the selected puromycin-positive clones, only clones in which the level of snoRNA was reduced by ~50% were identified, suggesting that double KO is most likely lethal (Figure 3Aii). The proper integration was examined by PCR using primers located in the insert, and upstream of snoRNA (Figure S3A). The level of Ψ guided by the snoRNA was determined by HydraPsiSeq, and reduction in the corresponding Ψ was observed, with no changes in the level of Ψ seen in the neighboring positions (Figure 3Aiii). The reduction in the level of the snoRNA and the consequent reduction in the level of Ψ affected cell growth, as can be seen by comparing the growth rate of sKO compared with the PS expressing the Cas9 protein (Figure S3B). The result of translation in both sKO cell lines indicated by methionine incorporation, showed a mild non-significant global effect on translation (Figure 3Aiv). The level of the ribosome subunits and polysomes

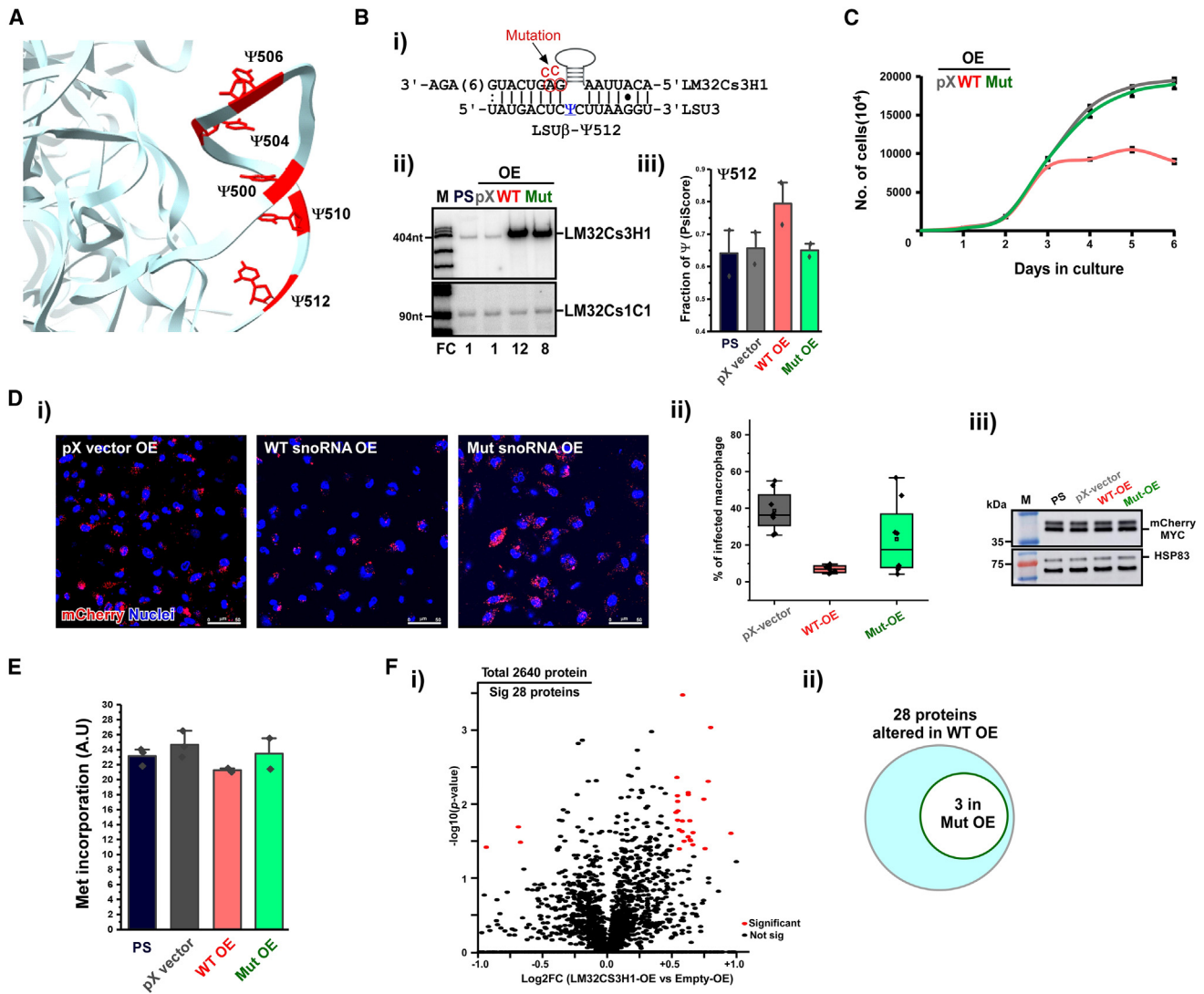


**Figure 2. Overexpression of LM32Cs3H1 snoRNA, guiding  $\Psi$ 512 on *Leishmania* LSU rRNA, regulates translation**

(A) Localization of  $\Psi$  sites on the H69 of the *Leishmania* ribosome. The positions of all five  $\Psi$  sites are indicated.

(B) Overexpression of LM32Cs3H1. (i) Schematic representation indicating potential base pairing of LM32Cs3H1 with the rRNA to guide  $\Psi$ 512, and the mutated form with two introduced mismatches (indicated in red). (ii) Validation of LM32Cs3H1 snoRNA overexpression by northern analysis.  $^{32}$ P-Labeled pBR322 DNA MspI digest was used as a size marker. (iii) LM32Cs3H1 snoRNA guides  $\Psi$ 512. PsiScore is presented. Data are presented as mean  $\pm$  SD. Experiments were done in duplicate ( $n = 2$ ).

(C) Growth of promastigote cells following LM32Cs3H1 overexpression. The growth of PS and overexpressing strains was compared at 27°C during the time period indicated. Data are presented as mean  $\pm$  SEM. Experiments were done in triplicate ( $n = 3$ ).

(D) Infection with *L. major* cells overexpressing LM32Cs3H1. (i) At 24 h post-infection, the percentage of macrophage cells hosting mCherry-expressing parasites was determined. The nuclei were stained with Hoechst. (ii) Box-plot representing the quantification of localization of mCherry in more than 100 cells per condition collected from more than five images. (iii) Whole cell lysates were prepared from cells expressing mCherry tagged with MYC, separated on SDS-PAGE followed by western blot.

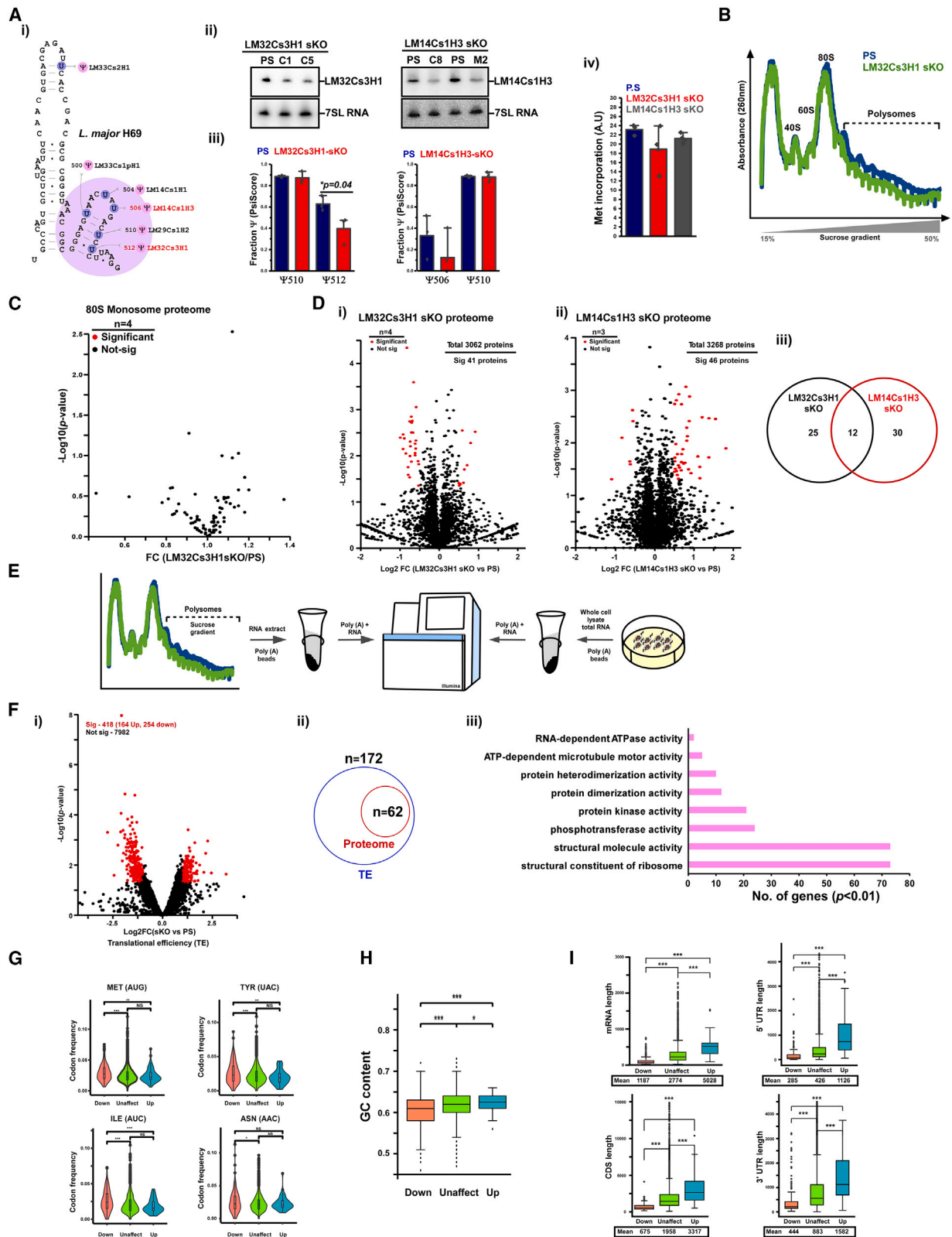
(E) Methionine incorporation assay. Data are presented as mean  $\pm$  SD of FITC intensity.

(F) Quantitative proteome of LM32Cs3H1 overexpression. (i) Data are presented as  $\log_2$ FC in the x axis, and  $-\log_{10}(p\text{ value})$  along the y axis. Significant changes in protein abundance are indicated by red dots, and non-significant changes are shown in black. (ii) Comparison of significantly altered proteins following overexpression of wild-type (WT) or mutated LM32Cs3H1 snoRNA.

were therefore examined by sucrose gradient fractionation and the results showed a slight decrease in the level of polyribosomes in sKO of LM32Cs3H1 (Figure 3B). However, no change was observed in the level of the ribosomal proteins in the purified

80S fraction, as determined by mass spectrometry (Figures 3C; Table S3).

To examine whether the change in the single snoRNA affected the translation of only a subset of proteins, we first checked if any



(legend on next page)

changes took place at the level of mRNA. To this end, we performed RNA-seq of poly(A)<sup>+</sup> selected RNA of the PS and compared it with the LM32Cs3H1 sKO cells. Approximately 8,400 mRNA species were identified in the libraries, but only 9 significant changes in mRNA level were observed in the LM32Cs3H1 sKO cells (Figures S3B; Table S4). Next, effects on specific translation were examined by determining the proteome using dimethyl labeling. Around 3,000 proteins were quantified, and the level of about 40 proteins was changed (Figure 3Di-ii; Table S5). The affected proteins observed in the two snoRNA sKO proteome experiments were distinct, and only 12 proteins were changed in both sKO (Figure 3Diii). With the exception of LmjF.23.1640, none of the proteins showed changes in mRNA abundance (Table S5). To validate that the differential proteome changes in LM32Cs3H1 sKO cells were due to the ablation of snoRNA and not to non-specific effects of CRISPR-Cas9, a wild-type snoRNA, a mutated version of the snoRNA, and empty pX-vector were transfected to the LM32Cs3H1 sKO cells (Figure S4A). As expected, the overexpression of wild-type snoRNA restored the level of  $\Psi$ 512 in LM32Cs3H1 sKO cells (Figure S4B). Interestingly, of the 24 proteins altered in LM32Cs3H1 sKO cells, the level of 13 proteins was restored upon addback expression of wild-type snoRNA, but only one protein was restored upon addback of the defective mutant snoRNA (Figure S4C), suggesting that, similar to overexpression cell lines (discussed above) most, however, not all of the phenotypes are an outcome of the altered ribosomes (see discussion).

Since proteome analysis is less sensitive compared with the identification of polysome-associated mRNAs, polysomal mRNAs were analyzed (Figure 3E). The association of the mRNA with polysomes was monitored and compared between the PS and sKO of LM32Cs3H1. The analysis revealed 164 and 254 mRNAs in which the polysome association was altered, i.e., increased or decreased, respectively (Figure 3Fi; Table S6). Among the mRNAs that were changed in polysomal association, the proteins corresponding to 172 mRNA were detected in the proteome analysis

and, of these, 62 proteins showed the same trend by both methods (Figure 3Fii). Inspecting the GO terms of the mRNAs whose translation was affected in sKO indicated that these belong to distinct families, proteins involved in the structure of the ribosomes, and to a lesser extent, proteins involved in signaling, including kinases (Figure 3Fiii). To explore why the translation of these mRNAs was affected, the codon compositions of these mRNAs were compared with unaffected mRNA molecules, and a significant difference was observed in individual codon frequency of these mRNAs relative to the unaffected mRNAs. Among mRNAs enriched in the polysomal fraction, eight codons (ACG, AGC, CCA, CCC, CCG, CCU, UCA, and UCG) were enriched, whereas, in mRNAs that were less abundant in polysomes, seven codons (AAC, AAG, AUC, AUG, CGC, GGT, and UAC) were enriched (Figures 3G and S5; Table S6). The codons of those mRNAs that are less abundant in polysomes had a lower GC content ( $p < 0.001$ ) compared with the rest of the mRNAs (Figure 3H). However, mRNAs whose abundance was enhanced in polysomes had longer ORFs, and 5' and 3' UTRs ( $p < 0.001$ ), whereas those whose abundance was decreased seemed to be shorter in all mRNA parts ( $p < 0.001$ ) (Figure 3I). mRNAs that possess longer 5', especially 3' UTRs, are more tightly regulated in the cells,<sup>39</sup> suggesting that  $\Psi$  on H69 may contribute to translational regulation, as described below.

### High-resolution cryo-EM structure of *L. major* 80S ribosomes

To understand the structural implication of  $\Psi$ 512 on the ribosome, we studied the 3D structure of *L. major* ribosomes using cryo-EM. Intact vacant 80S ribosomes were purified from cells expressing Cas9 (PS), and from LM32Cs3H1 sKO cells and subjected to cryo-EM data collection. The initial dataset included 377,797 and 345,376 particles for the PS and the LM32Cs3H1 sKO, respectively, yielding a 2.81 and 2.96 Å reconstructions of their 80S ribosomes, respectively (Figure S6). Upon several rounds of 3D classification, Bayesian polishing, and refinement, we improved the EM

### Figure 3. Depletion of snoRNA guiding $\Psi$ on *Leishmania* LSU rRNA regulates translation

(A) CRISPR-Cas9 knockout of *L. major* snoRNA. (i) Scheme indicating the identity of snoRNA guiding  $\Psi$  sites on the H69. (ii) Validation of single KO (sKO) of snoRNA by northern analysis. (iii) LM32Cs3H1 and LM14Cs1H3 snoRNA guides  $\Psi$ 512 and  $\Psi$ 510, respectively. PsiScore is presented. Data are presented as mean  $\pm$  SD.  $p$  value was determined by Student's  $t$  test. Experiments were done in triplicate ( $n = 3$ ). (iv) Methionine incorporation assay. Data are shown as mean  $\pm$  SD of FITC intensity. (B) Fractionation of ribosomes on a sucrose gradient. The fractions containing 40S, 60S, and 80S monosomes, and polysomes are indicated. (C) Composition of 80S monosomes. Data are presented as FC in the x axis and  $-\log_{10}(p \text{ value})$  along the y axis. Significant changes in protein abundance are indicated by red dots and non-significant changes in black. (D) Quantitative proteome of snoRNA sKO cells. Whole-cell lysates were labeled with dimethyl isotopes and subjected to mass spectrometry. (i) LM32Cs3H1, (ii) LM14Cs1H3. Data are presented as  $\log_2\text{FC}$  in the x axis and  $-\log_{10}(p \text{ value})$  along the y axis. Significant changes in protein abundance are indicated by red dots, and non-significant changes are shown in black. (iii) Venn diagram illustrating the comparison of significantly altered proteins following LM32Cs3H1 sKO and LM14Cs1H3 sKO. (E) Polysome profiling. Diagram indicating the polysome profiling protocol used in this study. (F) Differentially translated mRNAs. Translation efficiency (TE) was calculated using DTEG.R.<sup>60</sup> (i) TE of mRNAs was calculated for PS and LM32Cs3H1 sKO. Data are presented as  $\log_2\text{FC}$  (sKO/PS) in the x axis and  $-\log_{10}(p \text{ value})$  along the y axis. Significant changes in mRNA abundance are indicated by red dots, and non-significant changes are shown in black. (ii) Comparison of significantly altered mRNA and proteins following LM32Cs3H1 sKO. (iii) Gene ontology of mRNAs differentially translated upon LM32Cs3H1 sKO. (G) Codon usage of mRNAs whose translation was affected upon LM32Cs3H1 sKO. The deregulated mRNAs were classified as downregulated (down), upregulated (up) and unaffected (unaffected). The Wilcoxon test was calculated to estimate the  $p$  value. \* $p \leq 0.05$ , \*\* $p \leq 0.01$ , \*\*\* $p \leq 0.001$ ; NS, not significant. Representative box-plots of four codons are presented. The complete box-plots of all codons are presented in Figure S5. (H) GC content of mRNAs for the differentially affected mRNA. The mean length is indicated. Significant differences were plotted using the Wilcoxon test (\* $p \leq 0.05$ , \*\* $p \leq 0.01$ , \*\*\* $p \leq 0.001$ ) in the ggsignif (v.0.6.4) package (<https://const-ae.github.io/ggsignif/>). (I) The length of different mRNA domains. Comparison for the lengths of various mRNA domains of the differentially expressed mRNAs is presented. The mean length of each domain is indicated. Wilcoxon test was calculated as in (H).

maps to 2.4 Å (PDB: 8OVJ) and 2.46 Å (PDB: 8A98) resolution, respectively (Figure S6). Multibody refinement enabled to improve the resolution of head and body regions of the SSU (Figure S6). Inspection of the resulting map indicated that the H69 was visible in the sKO and the PS maps. The final EM map enabled us to build, refine, and model all nine rRNA fragments (SSU, the two LSU fragments [LSU $\alpha$  and  $\beta$ ], 5.8S, srRNA 1, 2, 4, 6, and 5S), E-site tRNA alongside 40 and 32 RP (ribosomal protein) in LSU and SSU, respectively (Figures 4A and S7; Tables S7 and S8). Note, our cryo-EM structure analyses detected all RP previously reported in *Leishmania* (PDB: 6AZ1 and 6AZ3) and *Trypanosoma brucei* (PDB: 80VA and 80VE) ribosomes and did not reveal any additional ribosomal proteins. The final *L. major* vacant 80S ribosome model is highly similar to the previously published *L. donovani* ribosome (PDB: 3JCS, 6AZ1, and 6AZ3) with minor rRNA and RP conformational changes.<sup>40,41</sup>

Previous structural and mass spectrometry studies in *L. donovani* suggested that *Leishmania* ribosomes harbor several unique and conserved rRNA modifications.<sup>40–42</sup> The high-resolution structures presented here enabled us to model and visualize 97 2'-O-methylation sites, 8 base modifications including m<sup>1</sup>A, m<sup>6</sup><sub>2</sub>A, m<sup>5</sup>C, m<sup>7</sup>G, m<sup>1</sup>acp $\Psi$ , and 49  $\Psi$  residues (Figures 4B and S8; Table S9). Among these, 74 Nms are conserved between *L. major*, *L. donovani*, and *T. brucei*, whereas 22 Nms are species-specific modifications. The  $\Psi$  positions were modeled based on the 49  $\Psi$ s that were visualized, and the remaining 15  $\Psi$  based on  $\Psi$ -seq and HydraPsiSeq (Figure 4C). Of note, the vacant 80S ribosome map resolution at the H69 region was not sufficient to model  $\Psi$  nucleotides. To obtain a sequencing independent detection of  $\Psi$  in *L. major* ribosomes, we determined the presence of  $\Psi$  using tandem LC-MS<sup>8,43</sup> (Table S10). LC-MS of purified rRNA subunits detected all  $\Psi$ s detected by  $\Psi$ -seq and HydraPsiSeq except SSU\_ $\Psi$ 33, SSU\_ $\Psi$ 1192, LSU $\alpha$ \_ $\Psi$ 239, LSU $\alpha$ \_ $\Psi$ 940, and LSU $\beta$ \_ $\Psi$ 1265. Tandem LC-MS analysis also detected six highly conserved rRNA modifications on H69, i.e.,  $\Psi$ 500, Am502,  $\Psi$ 504,  $\Psi$ 506,  $\Psi$ 510, and  $\Psi$ 512, that we previously described to exist in *T. brucei*<sup>43</sup> (Table S10).

We superimposed both structures to investigate the structural differences between PS and ribosomes lacking  $\Psi$ 512 (LM32Cs3H1 sKO). However, no significant global differences between the overall architecture were observed. The comparison of the *L. major* PS H69 with H69 of *L. donovani* (6AZ3) and *T. brucei* (4V8M) suggested a highly conserved and/or identical base pairing scheme (Figure S9). Upon closer inspection of H69 helices, we noticed that the density of H69 and h44 in PS vacant ribosomes was of better quality compared with the sKO ribosomes, suggesting that this region is highly flexible in the sKO (Figure S10). Thus, we were able to confidently model the entire H69 and h44 only in the PS and not in the sKO ribosomes.

Since H69 is known to be dynamic during different stages of translation,<sup>44</sup> we sought to reconstitute the post-decoding pre-translocation state (classical-PRE) *in vitro*.<sup>45,46</sup> The *L. major* classical-PRE-ribosome complex was formed by incubating vacant 80S monosomes with a pre-programmed synthetic mRNA fragment containing the leishmanial Kozak sequence<sup>47</sup> in its 5' termini followed by AUG-UUC codons, *E. coli* P-site tRNA encoding for fMet-AUG codon, and an *E. coli* A-site tRNA encoding for Phe-UUC codon. Reconstructions of the classical-PRE-ribosome

complex from PS and sKO enabled us to obtain cryo-EM maps of  $\sim$ 3 Å resolution (PDB: 8RXH and 8RXX) (Figure S6). Cryo-EM mapping of the PS-PRE-ribosome enabled us to model all the three tRNAs, mRNA, as well as the entire H69 region (Figure 5A). The quality of the classical-PS-PRE-ribosome map also allowed us to model rRNA modifications such as Am502,  $\Psi$ 504,  $\Psi$ 510, and  $\Psi$ 512 in the H69 (Figure 5Bi). Similarly, the cryo-EM map of the classical-sKO-PRE-ribosome enabled us to confidently model the P- and E-site tRNAs, mRNA and H69 (Figure 5Bi), suggesting that H69 is stabilized in sKO in the classical-PRE compared with the vacant-80S monosomes. Of note, the EM-map of the classical-sKO-PRE-ribosome had poor density for A-site tRNA (Figure 5A). Multibody focused refinement using a separate mask for A/P-site tRNAs, SSU, and LSU enabled us to better model the nucleotides of A-site tRNA near the decoding site and H69 (Figure S6). Superimposing PS and sKO H69 suggested a similar overall architecture in the classical-PRE state (Figure 5Bii). The quality of both maps also allowed us to model  $\Psi$ 512, suggesting that  $\Psi$ 512 is detectable in our EM maps even if the one copy of the cognate snoRNA is deleted (Figure 5Bii). We were also able to model other  $\Psi$ s on H69 using the cryo-EM maps obtained from the classical-PRE-ribosome (Figure S11). Taken together, using all our cryo-EM maps, we were able to model 57  $\Psi$ s, 104 Nms, and 9 base modifications (Table S9).

Similar to other known ribosome structures,<sup>24</sup> in *Leishmania* ribosomes, H69 interacts with h44 of the SSU to form the B2a inter-subunit bridge (Figure 5C). To investigate the dynamics of h44 in PS ribosomes with and without mRNA-tRNAs, we superimposed PS-vacant-80S and PS-PRE-ribosome. The superimpositions revealed similar organization of H69 and h44 in both structures (Figures S12A and 12B). Closer inspection of the decoding region in PS ribosomes suggests that rRNA nucleotides A2158 and A2159 flip out of the h44 helical axis in the PS-PRE-ribosome as was previously indicated in mammalian and bacteria elongation complexes<sup>48</sup> (Figures 5D and S12C). Similarly, inspection of sKO-vacant-80S and sKO-PRE-ribosome complex suggests that the presence of mRNA and A/P-tRNAs stabilized the ribosome and resulted in a better quality cryo-EM map in this region that enabled us to confidently model H69 (Figure 5D). Next, we superimposed the PS and sKO PRE-ribosome and observed dual conformation of nucleotides H69-Am502 and h44-A2158 in the sKO ribosome (Figure 5E). Unlike PS-PRE-ribosome, the second conformation of Am502 (Am502b) nucleotide at the tip of H69 faces toward the h44. Similarly, the second conformation of A2158 (A2158b) is located within the helix as was seen in PS-vacant-80S-ribosomes (Figure 5E). Of note, in both PS and sKO-PRE-ribosome nucleotide A2159 is flipped out of the h44 helical axis. Interestingly, recent cryo-EM studies of yeast ribosomes lacking all rRNA  $\Psi$ s also observed two conformations in Am502 (A2256 in yeast) compared with wild-type ribosomes.<sup>49</sup> Thus, in sKO cells we observed a mixed population of PRE-ribosomes that partially resembles PS as well as an altered conformation, reflecting the cell being a sKO of LM32Cs3H1.

### Functional implication of $\Psi$ 512 on aminoglycoside antibiotic sensitivity

The structural analysis of PS and LM32Cs3H1 sKO ribosomes suggested that H69 and h44 undergo structural changes in the

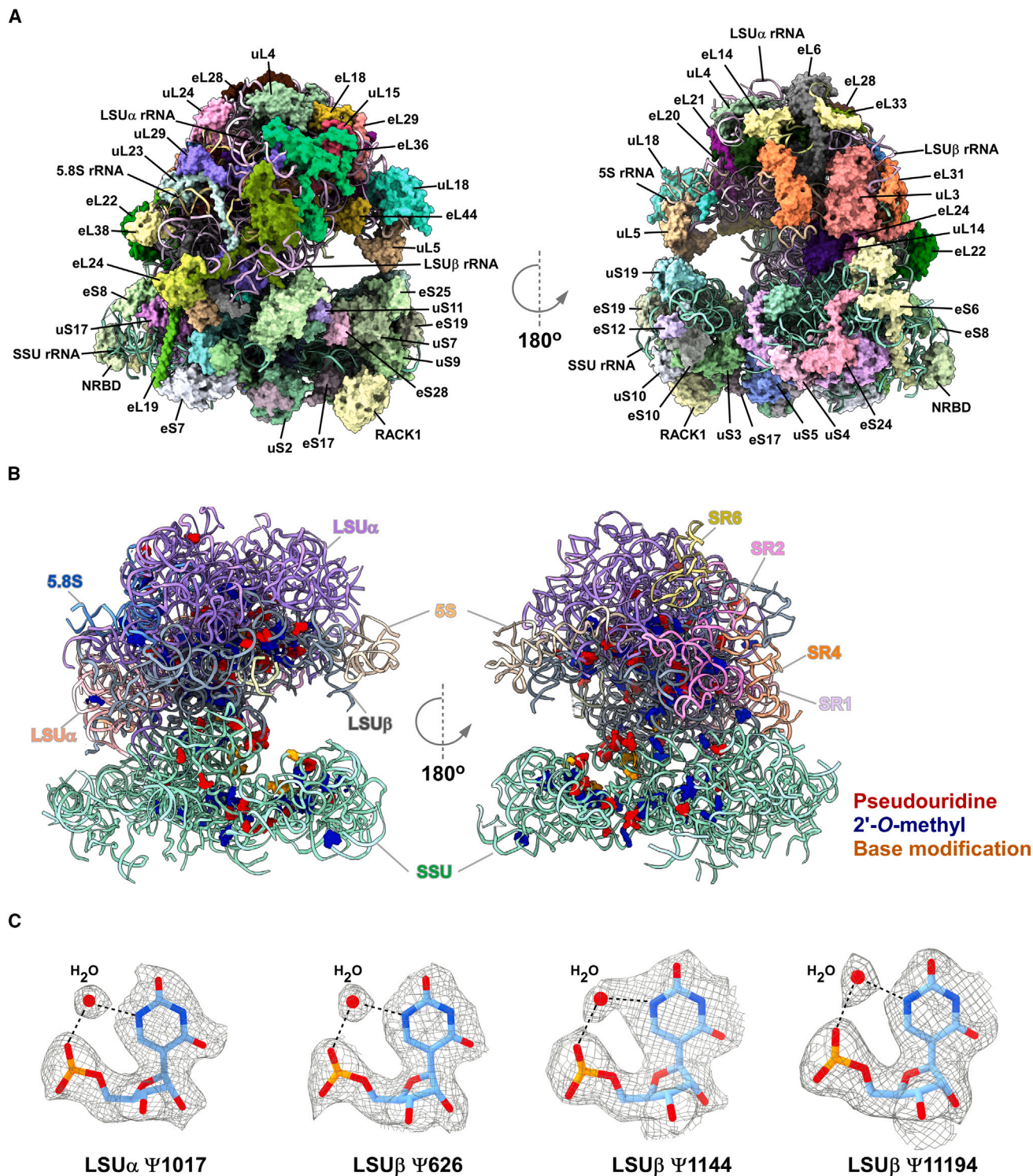
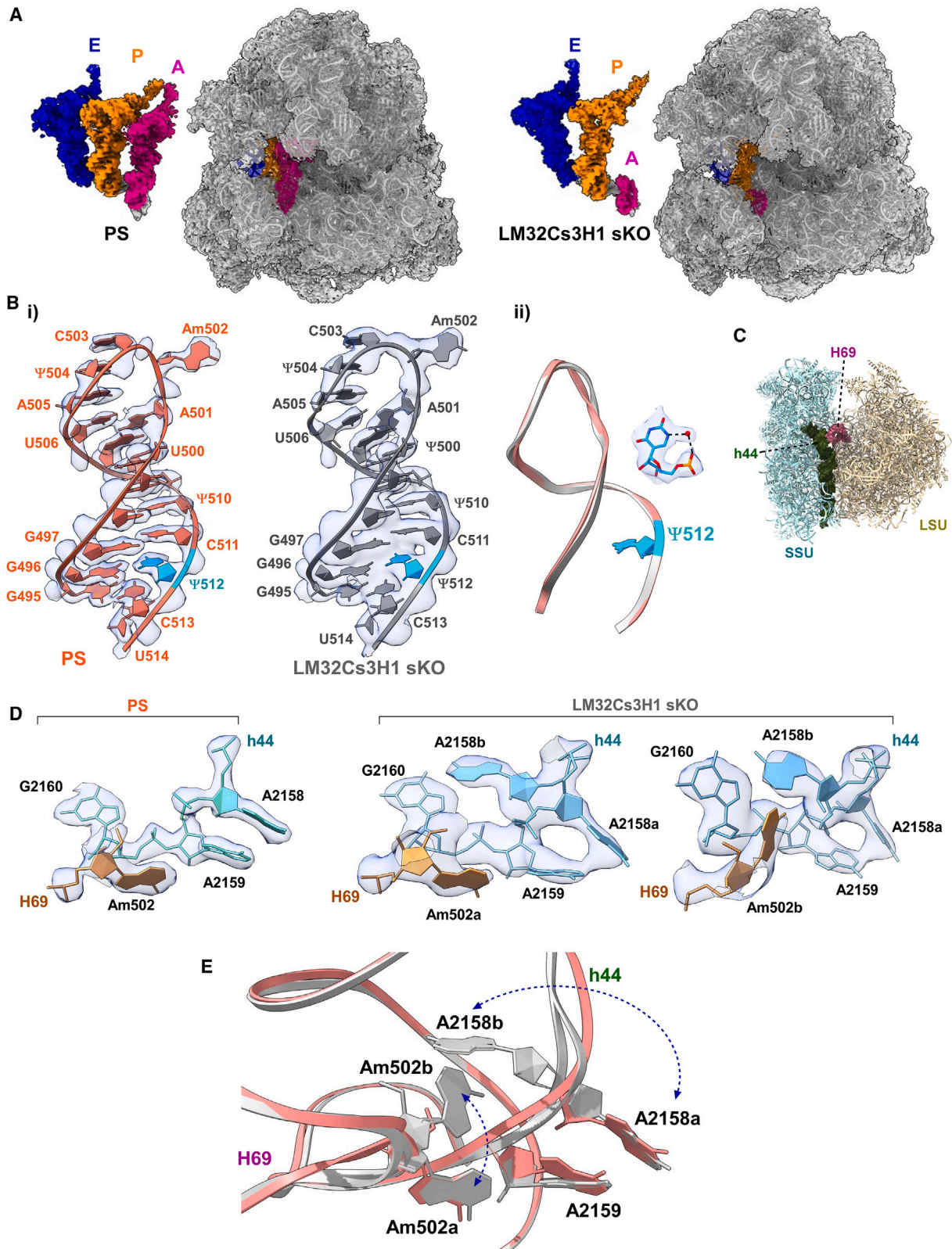


**Figure 4. High-resolution cryo-EM structure of *L. major* vacant-80S ribosome at 2.4 Å**

(A) The atomic structure of *L. major* ribosome. The atomic structure is shown in both front and back views. The different protein chains are shown in a space filled presentation by various colors, and the various RNA chains are shown as ribbons.

(B) Location of rRNA modifications in the *L. major* ribosome.  $\Psi$ , 2'-O-methylations and base-modifications are presented in red, blue, and orange, respectively.

(C) Examples of  $\Psi$  visualized in cryo-EM map by contacts with water molecules. The cryo-EM map and the corresponding model are superimposed. The identity of  $\Psi$  residues is given. Dotted lines indicate the potential hydrogen bonds between the water molecules and the N1-atom of the  $\Psi$  nucleotides.



(legend on next page)

absence of  $\Psi$ 512 (Figures 5 and S10). We therefore envisioned that such a rearrangement could influence the binding of aminoglycosides. Aminoglycosides are broad-spectrum antibiotics that bind to the major groove of h44 in the SSU rRNA.<sup>50,51</sup> The binding site of aminoglycosides is highly conserved between bacteria (*E. coli*), yeast, human, and *Leishmania* (Figure 6A).<sup>40</sup> To study the effect of  $\Psi$ 512 sKO on cell growth following aminoglycoside treatment, we selected G418 (geneticin), which belongs to the family of 2-deoxystreptomycin (2-DOS) ring-containing aminoglycosides.<sup>51</sup> The growth of PS and LM32Cs3H1 sKO cells treated with various concentrations of G418 was monitored (Figure 6B). LM32Cs3H1 sKO cells exhibited reduced sensitivity to G418 compared with PS (Figure 6B). To explore the underlying mechanism, we conducted a comparative analysis of the *L. major* 80S ribosome structures and yeast ribosome bound to G418 (PDB: 5NDG) (Figure 6C). In yeast, G418 binding is stabilized by a stacking interaction with nucleotide A2157 (A1754 in yeast) and by the flipping out of nucleotides A2158 and A2159 (A1755 and A1756 in yeast, respectively) (Figure 6C). These flipped-out nucleotides are positioned in proximity to the tip of H69 (~4 Å from A502 [A2256 in yeast]). The structural superposition of our high-resolution structure of PS ribosomes allowed us to model this interaction in *L. major* (Figure 6D). Our PS ribosome structure was reconstructed using native 80S ribosome state in the absence of G418, and therefore we observed that nucleotides A2158 and A2159 are within the helical axis and may potentially be displaced upon binding with G418, as seen in the yeast ribosome (PDB: 5NDG) (dashed lines with an arrow indicate the flipping-out movement). To understand the mechanism of reduced sensitivity in LM32Cs3H1 sKO cells, we sought to test the inhibitory activity of G418 *in vitro* using lysates prepared from PS and sKO cells. Cell-free transcription and translation assay using S12 lysates (Figure 6E) demonstrated that both PS and sKO lysates translate the leaderless green fluorescent protein (GFP) mRNA similarly in the presence of varying G418 concentration, suggesting that the loss of  $\Psi$ 512 does not affect G418 binding in the ribosomes. In contrast, sucrose gradient fractionation of sKO lysates demonstrated decreased level of polyribosomes (Figure 3B) compared with the PS, suggesting that LM32Cs3H1 sKO cells might be less sensitive to G418 owing to defects in ribosome formation or other factors such as transport of G418 into the cell. Thus, the lack of  $\Psi$ 512 could potentially be exploited by *Leishmania* parasites to develop aminoglycoside resistance.

### A proposed model explaining the preferential translation of mRNA carrying codon bias

Our data (Figures 3G and S5; Table S6) indicate that the translation efficiency of mRNAs with distinct codon bias was altered in

the sKO. Previous studies described a similar phenomenon following changes in specific rRNA 2'-O-methylation, but the mechanism connecting the modification with the effect on translation remained unknown.<sup>52</sup> Moreover, our EM-maps of reconstituted sKO-PRE-ribosome failed to observe good density in the A-site tRNA (Figure 5A). Based on our high-resolution structure and polysome profiling, we propose a mechanism by which specific codons are preferentially chosen in sKO cells lacking  $\Psi$ 512. The comparison of *L. major* PS-PRE-ribosome and *L. donovani* 80S structure (PDB: 6AZ1 and 6AZ3)<sup>40</sup> suggests that the tip of H69, A502 is in close proximity to the A-site tRNA's 4th, 5th, and 6th nucleotide downstream (5'-3') from the tRNA anticodon (Figure 7A) and could potentially affect tRNA decoding interaction with h44. Similar interactions could also be seen in cryo-EM structures of the human ribosomes in complex with A-site tRNA and mRNA (PDB: 8G6J). Structural studies of mammalian ribosomes suggested that h44 nucleotides A2158 and A2159 assist in inspecting the geometry of the codon-anticodon helix and stabilize A-site tRNA by hydrogen bonding.<sup>48</sup> Thus, such interaction might be selectively affected in the sKO cells due to flexibility at the H69 tip (A502) and h44-A2158 hindering A-site tRNA interactions. Indeed, deletion studies of A502 (A1913 in *E. coli*) in the tip of H69 resulted in a non-functional *E. coli* ribosome,<sup>53</sup> further supporting the importance of A502 for the proper function of the *Leishmania* ribosome. To further investigate the efficiency of sKO ribosomes to bind tRNAs, we purified tRNAs from translating polysome fraction and subjected them to tRNA-seq using the thermostable group II intron reverse transcriptase.<sup>14</sup> Our analysis detected the existence of 83 tRNAs encoding for 42 unique codons (Table S11). The results suggest that tRNAs coding for 12 different codons were significantly reduced in the sKO ribosomes (Figure S13; Table S11). Interestingly, the tRNA coding for Phe-UUC was significantly ( $p < 0.05$ ) reduced by 2.6-fold in the sKO ribosomes, suggesting that both *L. major* and *E. coli* tRNAs encoding for Phe-UUC codons bind with a lower affinity to the sKO ribosome. Notably, for codons such as AUG (Met) and UAC (Tyr), which are significantly enriched in mRNAs that are poorly translated in sKO cells (Figure 3G), their cognate tRNAs are significantly reduced in the sKO ribosomes, suggesting that mRNAs carrying these codons are poorly translated because their cognate tRNAs are poorly bound in sKO ribosomes. Whereas for codons such as AAC and AAG that are also significantly enriched in mRNAs that are poorly translated in sKO cells, we noticed a reduction in their cognate tRNA, but their  $p$  value was not significant. Note, the tRNA encoding for codons such as AUC, CGC, and GGU that were enriched in mRNAs that are poorly translated were not identified in this study.

### Figure 5. The atomic structure of H69 in ribosomes lacking $\Psi$ 512 in the classical-PRE-ribosome

(A) Cryo-EM map and model of PS and LM32Cs3H1 sKO classical-PRE-ribosomes. An enlarged inset of the density of all three tRNA is presented. A-, P-, and E-tRNAs are colored with pink, orange, and blue, respectively.

(B) Structure of the H69 in the classical-PRE-ribosome. (i) The cryo-EM density and base pairing scheme of the H69 in the PS and sKO ribosome. The identity of nucleotides is shown. PS and sKO nucleotides are represented in orange and gray, respectively.  $\Psi$ 512 is highlighted in cyan. (ii) Superimposition of H69 from PS and sKO ribosomes. A representative cryo-EM density for  $\Psi$ 512 is presented.

(C) The location of h44 and H69 in the *L. major* ribosome with respect to the SSU and LSU.

(D) The cryo-EM density of nucleotides at the tip of H69 and adjacent nucleotides in h44 is presented for PS (left) and sKO (right) ribosome.

(E) Superimposition of h44 and H69 from PS and LM32Cs3H1 sKO ribosomes. rRNA chains from PS and sKO are presented as orange and gray ribbons, respectively. Dotted lines indicate the potential flip between the dual conformations of the indicated nucleotides.

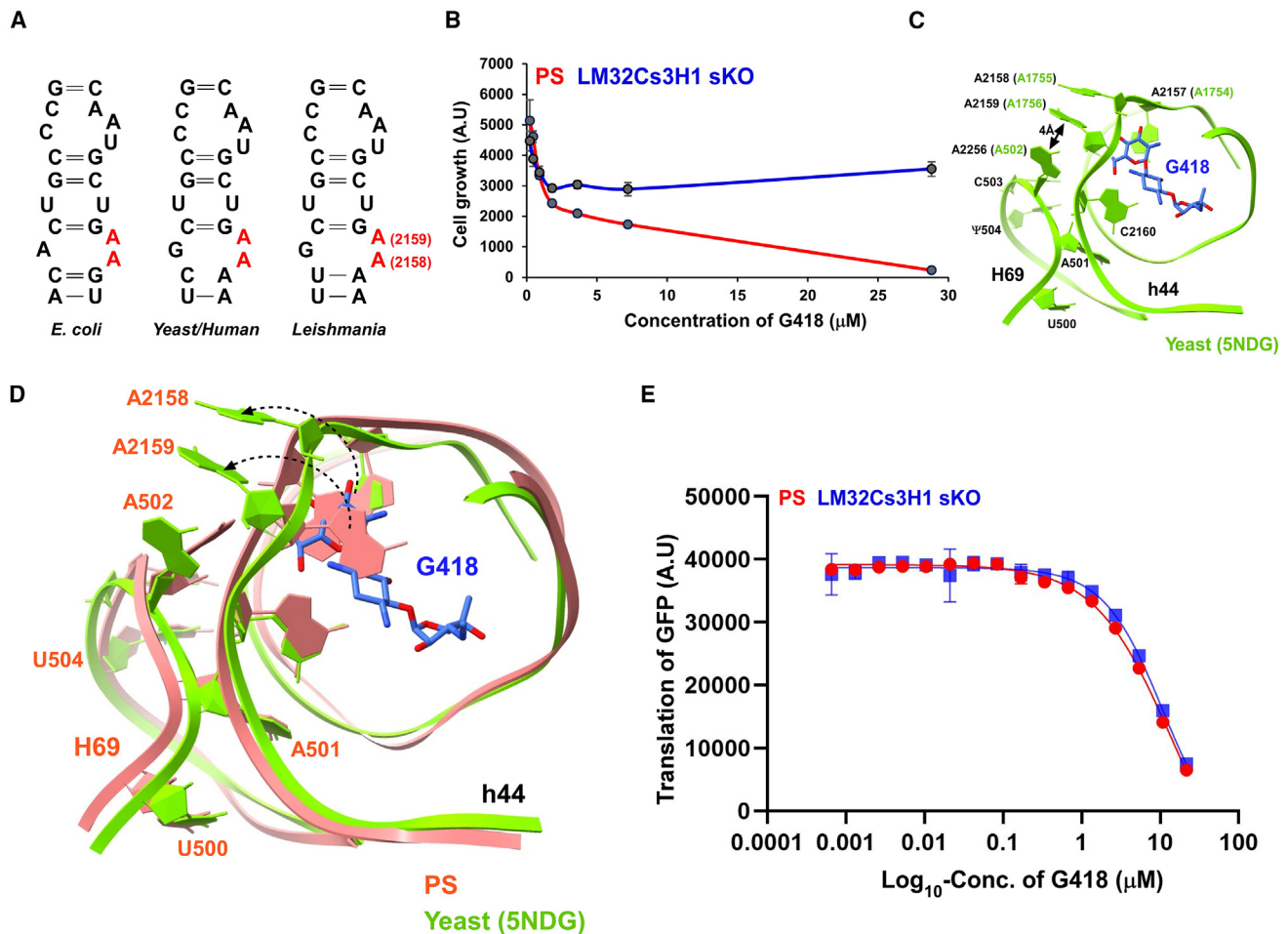


**Figure 6. G418 sensitivity of *Leishmania* cells lacking Ψ512**

(A) A conserved 2-DOS aminoglycoside binding site across species. The secondary structure of rRNA nucleotides around the aminoglycoside binding pocket is presented.

(B) Growth of promastigote cells incubated with G418. The growth of PS and LM32Cs3H1 sKO strains was compared at 27°C. Data are presented as mean ± SEM. Experiments were done in triplicate ( $n = 3$ ).

(C) The binding site of G418 in the yeast 80S ribosome. The nucleotides surrounding G418 in h44 and H69 are indicated in the yeast ribosome (PDB: 5NDG). The nomenclature of *L. major* nucleotides is presented, and the yeast homolog is shown in parentheses.

(D) Docking of G418 into *L. major* vacant 80S ribosomes. The structures of *L. major* PS (PDB: 8OVJ, shown in orange) and yeast ribosomes (shown in green) are superimposed and the docked location of G418 is shown. The direction of base flipping is shown by dotted lines with an arrowhead.

(E) *In vitro* translation assay using *L. major* S12 lysate. Data are presented as mean ± SD. A representative dose-response curve is presented.

Moreover, sequence comparison of specific tRNA isoacceptors of *L. major* proline, glycine, isoleucine, and alanine, which are reduced in sKO ribosomes, suggested that the 6th nucleotide (numbered from the anticodon) is variable among these isoacceptors (Figure 7B). Similarly, in isoleucine, the 4th nucleotide differs from the other isoacceptor (Figure 7B). This variability among these different isoleucine tRNA isoacceptors might affect their incorporation into the ribosomes in a manner dependent on interaction with the tip of H69 and h44-A2158. Interestingly, mutation analysis of *E. coli* H69 loop nucleotide A1913U (A502 in *L. major*) affected the incorporation of tRNA encoding specific codons such as AUA (isoleucine) during peptide formation.<sup>28</sup> Thus, we propose a mechanism in which the flexibility in the

H69 tip and h44-A2158, caused by the absence of Ψ512, leads to alteration in the interaction with specific tRNA sequences, preventing the incorporation of tRNAs that are essential for the translation of mRNAs harboring these unique codons (Figure 7C).

## DISCUSSION

This study demonstrates that, in the absence of a single specific Ψ in H69, the architecture of the entire helix is distorted. This change affects the translation of only a subset of proteins, whereas the translation of the majority of the mRNAs is not affected, suggesting that the Ψ modification contributes to a

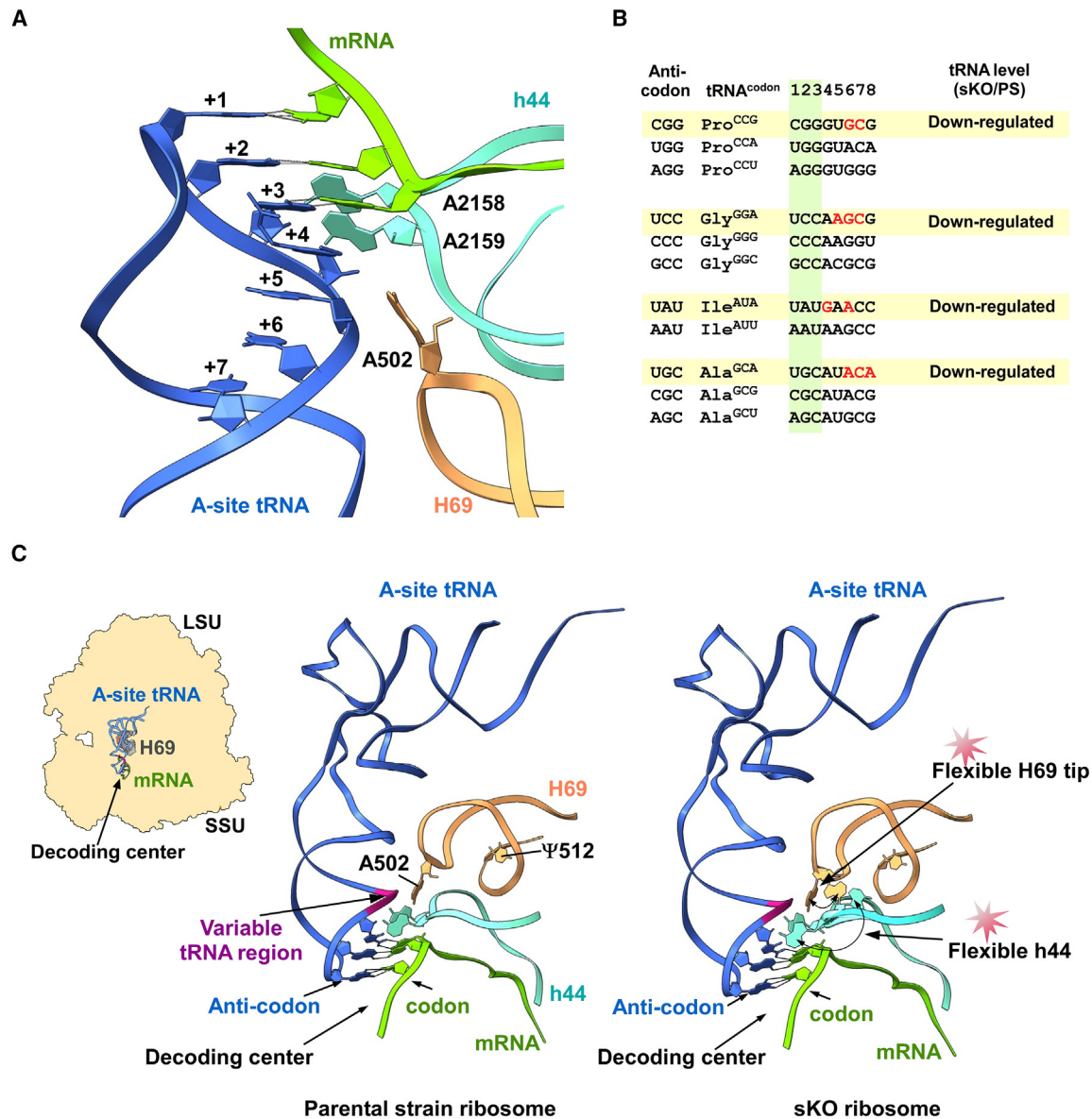


**Figure 7. Proposed mechanism for tRNA selectivity**

(A) A representative snapshot of the decoding region. The nucleotides in codon-anticodon base-pairing are indicated (nucleotides +1, +2, and +3). A-site tRNA, mRNA, H69, and h44 from PS-PRE-ribosome are shown as blue, green, orange, and cyan ribbons, respectively. The numbering of tRNA nucleotides, counted from the anticodon, is shown.

(B) Variability in specific tRNA sequence. The nucleotide sequence alignment of selected tRNA isoacceptors, highlighting the sequence variations in red. The numbering of nucleotides, counted from the anticodon loop, is shown in (A). The differential expression status of tRNAs from tRNA-seq data is indicated.

(C) Schematic overview illustrating the proposed mechanism for tRNA selectivity of ribosome carrying  $\Psi$ 512 in H69. The location of A-site tRNA, decoding center, H69 and h44 are indicated. The variable region of tRNA is indicated in dark pink. The nucleotides with dual conformation are indicated with black arrows.

cohort of heterogeneous ribosomes that may have diverse functions.

Our previous studies identified  $\Psi$  and Nm sites that are developmentally regulated between the *T. brucei* bloodstream form, which multiplies in the mammalian host, and the procyclic form, which proliferates in the insect.<sup>14,16,33</sup> Interestingly, with the exception of  $\Psi$ 512, the hyper- and hypomodified sites (in amastigotes vs. promastigotes) described in this study are not

located in functional domains (Figure 1; Table S1). Moreover, the altered sites are different from the sites observed on rRNA obtained from culture-adapted *L. donovani*, which proliferates faster than the population from which these originated.<sup>54</sup> Longer culture adaptation resulted in changes in Nm modification in the PTC and polypeptide entrance tunnel and  $\Psi$  in the PTC, suggesting that changes in rRNA modification contribute to the formation of ribosomes that promote the translation of mRNAs that

help acquire fitness gain.<sup>55</sup> We have recently demonstrated that sKO of homologous snoRNA guiding  $\Psi$ 512 in *Trypanosoma brucei* compromised growth and affected the translation of specific mRNAs.<sup>43</sup> The effect on translation was partially attributed to structural changes outside of H69 leading to the dislodging of eS12 RP located on the surface of the SSU ribosome. These studies highlight the function of individual  $\Psi$ s in functional domains that can potentially contribute to the generation of ribosomes selectively translating subsets of mRNAs.<sup>43</sup>

The current study supports the notion that an individual modification, even if present in a critical position such as H69, affects the translation of only a subset of proteins that have very specific biological functions (Figures 2 and 3). In yeast, it was necessary to change several  $\Psi$ s simultaneously to observe an effect on the translation efficiency and fidelity, while changing a single modification did not have any effect.<sup>20–22</sup> However, studies of cancer cells showed that reduction in expression of *SNORA24* guiding  $\Psi$  on SSU rRNA results in perturbations in tRNA selection and altered pre-translocation complex dynamics.<sup>56</sup> The effect of single rRNA modification was recently demonstrated for Nm modification. Ribosomes lacking snoRNA *SNORD45C*, which guides Nm in position Cm174 of human SSU rRNA, preferentially affected the translation of hundreds of mRNAs that differ in their nucleotide content.<sup>52</sup> In this study, we demonstrate that the most characteristic change in all mRNAs that were poorly translated is their short size in all domains. mRNAs that possess longer UTRs are known to be tightly regulated.<sup>39</sup> It is plausible that mRNAs that lack this kind of regulation are controlled by the intrinsic properties of CDS such as codon usage as demonstrated in this study. Such regulation could be manifested by the availability of tRNAs and their modification affecting their incorporation to ribosomes.

Why is the level of  $\Psi$ 512 on H69 so essential and has such a profound effect on H69 structure? The cryo-EM structure of yeast ribosome lacking  $\Psi$ s suggests that the modification on H69 may play a role in the movement of the ribosome's "head."<sup>23</sup> The finding that  $\Psi$ 512 is differentially regulated in three *Leishmania* species supports the importance of this specific modification for the function of the ribosome.

Our previous studies suggested that aminoglycosides bind to the *Leishmania* ribosome in the same location, with their conserved 2-DOS ring serving as a central anchor leading to misincorporation of tRNAs during translation.<sup>40</sup> The mechanism proposed in this study suggests that *Leishmania* parasites could utilize pseudouridylation in H69 rRNA (especially  $\Psi$ 512) as a strategy to overcome antibiotic stress during infection by compromising translation of specific mRNAs. Indeed, our recent structural studies using ribosomes isolated from aminoglycoside-resistant clinical isolates of *Pseudomonas aeruginosa* revealed unique changes in H69 conformation that could affect the proper formation of the intersubunit bridge (B2a).<sup>57</sup>

In this study we show that sKO of snoRNA guiding on  $\Psi$ 512 affect the translation of subset of mRNA carrying codon bias. We present evidence that the poor translation of mRNA with codon bias stems from the inability of the sKO ribosomes to properly bind specific tRNAs. Support to our proposal comes from studies in *E. coli* where the AUA codon that is decoded by tRNA<sup>Ile(UAU)</sup> carries two RNA modifications, one t6A in

the +4 nucleotide and  $\Psi$  in the +6 nucleotide from the anticodon.<sup>58,59</sup> Indeed, the *Leishmania* tRNA<sup>Ile(UAU)</sup> that is reduced in sKO ribosomes differs from well-accommodated isoacceptor in the same +4 and +6 positions. Interestingly, we mapped potential sites of tRNA modification in *L. major* (Figure S14) and found that tRNA<sup>Ile(UAU)</sup> possess an unknown modification at +4 position. This modification does not exist in the tRNA<sup>Ile(AAU)</sup> suggesting that the  $\Psi$  modification on rRNA is essential for incorporation of tRNA with specific modification like tRNA<sup>Ile(UAU)</sup>. Thus, the presence of tRNA modification in +4 nucleotide could potentially explain why a such modified tRNA requires proper contact with the H69 tip and h44 for its incorporation.

The mechanism proposed here to explain the translation effect on mRNAs with a particular codon bias provides a potential explanation to the long-standing question regarding the selective effect on translation of only a subset of mRNAs that have characteristic codon bias. We suggest that this effect is due to the defective selection of specific tRNAs by the ribosomes lacking  $\Psi$  modification.

Altogether, this study highlights the importance of a single specific  $\Psi$  modification for cell viability due to a specific effect on translation emerging from distinct structural changes in the ribosome. It seems that this observation could be harnessed for designing novel antisense therapies to inhibit snoRNA function.

### Limitations of the study

Our high-resolution structural analysis was capable of identifying a mixed population of ribosomes in the sKO cells. We could not easily separate ribosomes lacking or having a single  $\Psi$  because these changes did not affect the composition of the ribosomes. This goal can be only achieved if a very large cryo-EM micrographs dataset is collected and ribosomes without A-site tRNA are characterized in the sKO strain. Despite several attempt to create a double knockout for LM32Cs3H1, we could not obtain such viable cells. This most likely reflects the essentiality of snoRNAs for *Leishmania*.

### STAR★METHODS

Detailed methods are provided in the online version of this paper and include the following:

- KEY RESOURCES TABLE
- RESOURCE AVAILABILITY
  - Lead contact
  - Materials availability
  - Data and code availability
- EXPERIMENTAL MODEL AND STUDY PARTICIPANT DETAILS
  - Animals and parasites
- METHOD DETAILS
  - Generation of transgenic *L. major* parasites
  - Monitoring amastigote parasites within infected macrophages
  - Preparation of H/ACA snoRNome
  - Northern analysis
  - (N-cyclohexyl-N'-β-(4-methylmorpholinium) ethylcarbodiimide *p*-tosylate) treatment
  - $\Psi$ -seq and detection of pseudouridylated sites
  - Hydrazine and aniline treatment
  - HydraPsiSeq library preparation
  - HydraPsiSeq data analysis

- Proteolysis and dimethyl labeling
- Mass spectrometry analysis of proteins
- Methionine incorporation assay
- Translation efficiency and mRNA characteristics analysis
- Fractionation of ribosomes on sucrose gradient
- Purification of 80S ribosomes for cryo-EM
- Ternary 80S complex formation with mRNA and tRNAs
- Cryo-EM data collection and refinement
- Model building and refinement
- Purification of rRNA subunits
- LC-MS and MS/MS analysis and database search of RNA fragments
- Cell-free transcription-translation assay
- **QUANTIFICATION AND STATISTICAL ANALYSIS**

### SUPPLEMENTAL INFORMATION

Supplemental information can be found online at <https://doi.org/10.1016/j.celrep.2024.114203>.

### ACKNOWLEDGMENTS

This work was supported by a grant from the Israel Science Foundation (1959/20) to S.M.; ERC 2022-SYG DECOLeishRN grant to S.M., G.F.S., and Y.P.; the Agence Nationale pour la Recherche Labex “Integrative Biology of Emerging Infectious Diseases” contract ANR-10-LABX-62-IBEID and Labex “French Alliance for Parasitology and Health Care” contract ANR-11-LABX-0024 to G.F.S., E.P., and P.P.; the Kimmelman Center for Macromolecular Assemblies to A.Y.; and the Campus France Franco-Israeli Programme Hubert Curien Maimonide 2018 grant to S.M. and G.F.S. K.S.R. is supported by the Dean of Faculty Fellowship, Koshland Prize, and Sir Charles Clore Postdoctoral Fellowship from the Weizmann Institute. S.M. holds the David and Inez Myers Chair in RNA silencing of diseases. A.Y. holds the Martin S. and Helen Kimmel Professorial Chair at the Weizmann Institute of Science.

### AUTHOR CONTRIBUTIONS

Conceptualization, K.S.R. and S.M.; methodology, K.S.R., D.-G.H., M.O., E.P., P.P., M.T., Y.N., and S.C.-C.; validation, K.S.R. and A.B.; formal analysis, K.S.R., D.-G.H., A.B., S.A., H.M., A.F., T.B., M.T., and E.Z.; investigation, K.S.R. and A.B.; writing – original draft, K.S.R. and S.M.; writing – review & editing, K.S.R., A.B., G.F.S., A.Y., M.T., and S.M.; supervision and project administration, A.B., T.I., G.F.S., R.U., A.Y., and S.M.; funding acquisition, G.F.S., R.U., A.Y., and S.M.

### DECLARATION OF INTERESTS

The authors declare no competing interests.

Received: September 1, 2023

Revised: March 21, 2024

Accepted: April 23, 2024

Published: May 8, 2024

### REFERENCES

1. Burza, S., Croft, S.L., and Boelaert, M. (2018). Leishmaniasis. *Lancet* 392, 951–970. [https://doi.org/10.1016/S0140-6736\(18\)31204-2](https://doi.org/10.1016/S0140-6736(18)31204-2).
2. Ponte-Sucre, A., Gamarro, F., Dujardin, J.-C., Barrett, M.P., López-Vélez, R., García-Hernández, R., Pountain, A.W., Mwenechanya, R., and Papadopoulos, B. (2017). Drug resistance and treatment failure in leishmaniasis: A 21st century challenge. *PLoS Neglected Trop. Dis.* 11, e0006052. <https://doi.org/10.1371/journal.pntd.0006052>.
3. Séguin, O., and Descoteaux, A. (2016). Leishmania, the phagosome, and host responses: The journey of a parasite. *Cell. Immunol.* 309, 1–6. <https://doi.org/10.1016/j.cellimm.2016.08.004>.
4. Clayton, C.E. (2016). Gene expression in Kinetoplastids. *Curr. Opin. Microbiol.* 32, 46–51. <https://doi.org/10.1016/j.mib.2016.04.018>.
5. Clayton, C. (2013). The regulation of trypanosome gene expression by RNA-binding proteins. *PLoS Pathog.* 9, e1003680. <https://doi.org/10.1371/journal.ppat.1003680>.
6. Rajan, K.S., Doniger, T., Cohen-Chalamish, S., Rengaraj, P., Gallii, B., Aryal, S., Unger, R., Tschudi, C., and Michaeli, S. (2020). Developmentally Regulated Novel Non-coding Anti-sense Regulators of mRNA Translation in *Trypanosoma brucei*. *iScience* 23, 101780. <https://doi.org/10.1016/j.isci.2020.101780>.
7. Hoernes, T.P., and Erlacher, M.D. (2017). Translating the epitranscriptome. *Wiley Interdiscip. Rev. RNA* 8, e1375. <https://doi.org/10.1002/wrna.1375>.
8. Taoka, M., Nobe, Y., Yamaki, Y., Sato, K., Ishikawa, H., Izumikawa, K., Yamachi, Y., Hirota, K., Nakayama, H., Takahashi, N., and Isobe, T. (2018). Landscape of the complete RNA chemical modifications in the human 80S ribosome. *Nucleic Acids Res.* 46, 9289–9298. <https://doi.org/10.1093/nar/gky811>.
9. Kiss-László, Z., Henry, Y., Bachelier, J.P., Caizergues-Ferrer, M., and Kiss, T. (1996). Site-specific ribose methylation of preribosomal RNA: a novel function for small nucleolar RNAs. *Cell* 85, 1077–1088. [https://doi.org/10.1016/S0092-8674\(00\)81308-2](https://doi.org/10.1016/S0092-8674(00)81308-2).
10. Ganot, P., Bortolin, M.L., and Kiss, T. (1997). Site-specific pseudouridine formation in preribosomal RNA is guided by small nucleolar RNAs. *Cell* 89, 799–809. [https://doi.org/10.1016/S0092-8674\(00\)80263-9](https://doi.org/10.1016/S0092-8674(00)80263-9).
11. Ni, J., Tien, A.L., and Fournier, M.J. (1997). Small nucleolar RNAs direct site-specific synthesis of pseudouridine in ribosomal RNA. *Cell* 89, 565–573. [https://doi.org/10.1016/S0092-8674\(00\)80238-x](https://doi.org/10.1016/S0092-8674(00)80238-x).
12. Kierzek, E., Malgowska, M., Lisowiec, J., Turner, D.H., Gdaniec, Z., and Kierzek, R. (2014). The contribution of pseudouridine to stabilities and structure of RNAs. *Nucleic Acids Res.* 42, 3492–3501. <https://doi.org/10.1093/nar/gkt1330>.
13. Charette, M., and Gray, M.W. (2000). Pseudouridine in RNA: what, where, how, and why. *IUBMB Life* 49, 341–351. <https://doi.org/10.1080/152165400410182>.
14. Rajan, K.S., Adler, K., Doniger, T., Cohen-Chalamish, S., Aharon-Hefetz, N., Aryal, S., Pilpel, Y., Tschudi, C., Unger, R., and Michaeli, S. (2022). Identification and functional implications of pseudouridine RNA modification on small noncoding RNAs in the mammalian pathogen *Trypanosoma brucei*. *J. Biol. Chem.* 298, 102141. <https://doi.org/10.1016/j.jbc.2022.102141>.
15. Rajan, K.S., Adler, K., Madmoni, H., Peleg-Chen, D., Cohen-Chalamish, S., Doniger, T., Gallii, B., Gerber, D., Unger, R., Tschudi, C., and Michaeli, S. (2021). Pseudouridines on *Trypanosoma brucei* mRNAs are developmentally regulated: Implications to mRNA stability and protein binding. *Mol. Microbiol.* 116, 808–826. <https://doi.org/10.1111/mmi.14774>.
16. Rajan, K.S., Doniger, T., Cohen-Chalamish, S., Chen, D., Semo, O., Aryal, S., Glick Saar, E., Chikne, V., Gerber, D., Unger, R., et al. (2019). Pseudouridines on *Trypanosoma brucei* spliceosomal small nuclear RNAs and their implication for RNA and protein interactions. *Nucleic Acids Res.* 47, 7633–7647. <https://doi.org/10.1093/nar/gkz477>.
17. Tusup, M., Kundig, T., and Pascolo, S. (2018). Epitranscriptomics of cancer. *World J. Clin. Oncol.* 9, 42–55. <https://doi.org/10.5306/wjco.v9.i3.42>.
18. Bellodi, C., McMahon, M., Contreras, A., Juliano, D., Kopmar, N., Nakamura, T., Maltby, D., Burlingame, A., Savage, S.A., Shimamura, A., and Ruggero, D. (2013). H/ACA small RNA dysfunctions in disease reveal key roles for noncoding RNA modifications in hematopoietic stem cell differentiation. *Cell Rep.* 3, 1493–1502. <https://doi.org/10.1016/j.celrep.2013.04.030>.
19. Yoon, A., Peng, G., Brandenburger, Y., Zollo, O., Xu, W., Rego, E., and Ruggero, D. (2006). Impaired control of IRES-mediated translation in X-linked dyskeratosis congenita. *Science* 312, 902–906. <https://doi.org/10.1126/science.1123835>.

20. King, T.H., Liu, B., McCully, R.R., and Fournier, M.J. (2003). Ribosome structure and activity are altered in cells lacking snoRNPs that form pseudouridines in the peptidyl transferase center. *Mol. Cell* 11, 425–435. [https://doi.org/10.1016/s1097-2765\(03\)00040-6](https://doi.org/10.1016/s1097-2765(03)00040-6).
21. Liang, X.h., Liu, Q., and Fournier, M.J. (2007). rRNA modifications in an intersubunit bridge of the ribosome strongly affect both ribosome biogenesis and activity. *Mol. Cell* 28, 965–977. <https://doi.org/10.1016/j.molcel.2007.10.012>.
22. Liang, X.-H., Liu, Q., and Fournier, M.J. (2009). Loss of rRNA modifications in the decoding center of the ribosome impairs translation and strongly delays pre-rRNA processing. *RNA* 15, 1716–1728. <https://doi.org/10.1261/rna.1724409>.
23. Zhao, Y., Rai, J., Yu, H., and Li, H. (2022). CryoEM structures of pseudouridine-free ribosome suggest impacts of chemical modifications on ribosome conformations. *Structure* 30, 983–992.e5. <https://doi.org/10.1016/j.str.2022.04.002>.
24. Yusupov, M.M., Yusupova, G.Z., Baucom, A., Lieberman, K., Earnest, T.N., Cate, J.H., and Noller, H.F. (2001). Crystal structure of the ribosome at 5.5 Å resolution. *Science* 292, 883–896. <https://doi.org/10.1126/science.1060089>.
25. Bashan, A., Agmon, I., Zarivach, R., Schlutzenzen, F., Harms, J., Berisio, R., Bartels, H., Franceschi, F., Auerbach, T., Hansen, H.A.S., et al. (2003). Structural basis of the ribosomal machinery for peptide bond formation, translocation, and nascent chain progression. *Mol. Cell* 11, 91–102. [https://doi.org/10.1016/s1097-2765\(03\)00009-1](https://doi.org/10.1016/s1097-2765(03)00009-1).
26. Yonath, A., and Bashan, A. (2004). Ribosomal crystallography: initiation, peptide bond formation, and amino acid polymerization are hampered by antibiotics. *Annu. Rev. Microbiol.* 58, 233–251. <https://doi.org/10.1146/annurev.micro.58.030603.123822>.
27. Ali, I.K., Lancaster, L., Feinberg, J., Joseph, S., and Noller, H.F. (2006). Deletion of a conserved, central ribosomal intersubunit RNA bridge. *Mol. Cell* 23, 865–874. <https://doi.org/10.1016/j.molcel.2006.08.011>.
28. Ortiz-Meoz, R.F., and Green, R. (2011). Helix 69 is key for uniformity during substrate selection on the ribosome. *J. Biol. Chem.* 286, 25604–25610. <https://doi.org/10.1074/jbc.M111.256255>.
29. White, T.C., Rudenko, G., and Borst, P. (1986). Three small RNAs within the 10 kb trypanosome rRNA transcription unit are analogous to domain VII of other eukaryotic 28S rRNAs. *Nucleic Acids Res.* 14, 9471–9489. <https://doi.org/10.1093/nar/14.23.9471>.
30. Campbell, D.A., Kubo, K., Clark, C.G., and Boothroyd, J.C. (1987). Precise identification of cleavage sites involved in the unusual processing of trypanosome ribosomal RNA. *J. Mol. Biol.* 196, 113–124. [https://doi.org/10.1016/0022-2836\(87\)90514-6](https://doi.org/10.1016/0022-2836(87)90514-6).
31. Rajan, K.S., Chikne, V., Decker, K., Waldman Ben-Asher, H., and Michaeli, S. (2019). Unique Aspects of rRNA Biogenesis in Trypanosomatids. *Trends Parasitol.* 35, 778–794. <https://doi.org/10.1016/j.pt.2019.07.012>.
32. Rajan, K.S., Zhu, Y., Adler, K., Doniger, T., Cohen-Chalamish, S., Srivastava, A., Shalev-Benami, M., Matzov, D., Unger, R., Tschudi, C., et al. (2020). The large repertoire of 2'-O-methylation guided by C/D snoRNAs on *Trypanosoma brucei* rRNA. *RNA Biol.* 17, 1018–1039. <https://doi.org/10.1080/15476286.2020.1750842>.
33. Chikne, V., Doniger, T., Rajan, K.S., Bartok, O., Eliaz, D., Cohen-Chalamish, S., Tschudi, C., Unger, R., Hashem, Y., Kadener, S., and Michaeli, S. (2016). A pseudouridylation switch in rRNA is implicated in ribosome function during the life cycle of *Trypanosoma brucei*. *Sci. Rep.* 6, 25296. <https://doi.org/10.1038/srep25296>.
34. Eliaz, D., Doniger, T., Tkacz, I.D., Biswas, V.K., Gupta, S.K., Kolev, N.G., Unger, R., Ullu, E., Tschudi, C., and Michaeli, S. (2015). Genome-wide analysis of small nucleolar RNAs of *Leishmania major* reveals a rich repertoire of RNAs involved in modification and processing of rRNA. *RNA Biol.* 12, 1222–1255. <https://doi.org/10.1080/15476286.2015.1038019>.
35. Marchand, V., Pichot, F., Neybecker, P., Ayadi, L., Bourguignon-Igel, V., Wacheul, L., Lafontaine, D.L.J., Pinzano, A., Helm, M., and Motorin, Y. (2020). HydraPsiSeq: a method for systematic and quantitative mapping of pseudouridines in RNA. *Nucleic Acids Res.* 48, e110. <https://doi.org/10.1093/nar/gkaa769>.
36. Xu, Y., Liu, L., Lopez-Estraño, C., and Michaeli, S. (2001). Expression studies on clustered trypanosomatid box C/D small nucleolar RNAs. *J. Biol. Chem.* 276, 14289–14298. <https://doi.org/10.1074/jbc.M007007200>.
37. Boersema, P.J., Raijmakers, R., Lemeer, S., Mohammed, S., and Heck, A.J.R. (2009). Multiplex peptide stable isotope dimethyl labeling for quantitative proteomics. *Nat. Protoc.* 4, 484–494. <https://doi.org/10.1038/nprot.2009.21>.
38. Beneke, T., Madden, R., Makin, L., Valli, J., Sunter, J., and Gluenz, E. (2017). A CRISPR Cas9 high-throughput genome editing toolkit for kinetoplastids. *R. Soc. Open Sci.* 4, 170095. <https://doi.org/10.1098/rsos.170095>.
39. Mayr, C. (2017). Regulation by 3'-Untranslated Regions. *Annu. Rev. Genet.* 51, 171–194. <https://doi.org/10.1146/annurev-genet-120116-024704>.
40. Shalev-Benami, M., Zhang, Y., Rozenberg, H., Nobe, Y., Taoka, M., Matzov, D., Zimmerman, E., Bashan, A., Isobe, T., Jaffe, C.L., et al. (2017). Atomic resolution snapshot of *Leishmania* ribosome inhibition by the aminoglycoside paromomycin. *Nat. Commun.* 8, 1589. <https://doi.org/10.1038/s41467-017-01664-4>.
41. Shalev-Benami, M., Zhang, Y., Matzov, D., Halfon, Y., Zackay, A., Rozenberg, H., Zimmerman, E., Bashan, A., Jaffe, C.L., Yonath, A., and Skiniotis, G. (2016). 2.8-Å Cryo-EM Structure of the Large Ribosomal Subunit from the Eukaryotic Parasite *Leishmania*. *Cell Rep.* 16, 288–294. <https://doi.org/10.1016/j.celrep.2016.06.014>.
42. Nakayama, H., Yamauchi, Y., Nobe, Y., Sato, K., Takahashi, N., Shalev-Benami, M., Isobe, T., and Taoka, M. (2019). Method for Direct Mass-Spectrometry-Based Identification of Monomethylated RNA Nucleoside Positional Isomers and Its Application to the Analysis of *Leishmania* rRNA. *Anal. Chem.* 91, 15634–15643. <https://doi.org/10.1021/acs.analchem.9b03735>.
43. Rajan, K.S., Madmoni, H., Bashan, A., Taoka, M., Aryal, S., Nobe, Y., Doniger, T., Galili Kostin, B., Blumberg, A., Cohen-Chalamish, S., et al. (2023). A single pseudouridine on rRNA regulates ribosome structure and function in the mammalian parasite *Trypanosoma brucei*. *Nat. Commun.* 14, 7462. <https://doi.org/10.1038/s41467-023-43263-6>.
44. Ali, I.K., Lancaster, L., Feinberg, J., Joseph, S., and Noller, H.F. (2006). Deletion of a Conserved, Central Ribosomal Intersubunit RNA Bridge. *Mol. Cell* 23, 865–874. <https://doi.org/10.1016/j.molcel.2006.08.011>.
45. Behrmann, E., Loerke, J., Budkevich, T.V., Yamamoto, K., Schmidt, A., Penczek, P.A., Vos, M.R., Bürger, J., Mielke, T., Scheerer, P., and Spahn, C.M.T. (2015). Structural Snapshots of Actively Translating Human Ribosomes. *Cell* 161, 845–857. <https://doi.org/10.1016/j.cell.2015.03.052>.
46. Bhaskar, V., Graff-Meyer, A., Schenk, A.D., Cavadini, S., von Loeffelholz, O., Natchiar, S.K., Artus-Revel, C.G., Hotz, H.-R., Bretones, G., Klaholz, B.P., and Chao, J.A. (2020). Dynamics of uS19 C-Terminal Tail during the Translation Elongation Cycle in Human Ribosomes. *Cell Rep.* 31, 107473. <https://doi.org/10.1016/j.celrep.2020.03.037>.
47. Lukes, J., Paris, Z., Regmi, S., Breitling, R., Mureev, S., Kushnir, S., Pyatkov, K., Jirků, M., and Alexandrov, K.A. (2006). Translational initiation in *Leishmania tarentolae* and *Phytomonas serpens* (Kinetoplastida) is strongly influenced by pre-ATG triplet and its 5' sequence context. *Mol. Biochem. Parasitol.* 148, 125–132. <https://doi.org/10.1016/j.molbiopara.2006.03.008>.
48. Shao, S., Murray, J., Brown, A., Taunton, J., Ramakrishnan, V., and Hegde, R.S. (2016). Decoding Mammalian Ribosome-mRNA States by Translational GTPase Complexes. *Cell* 167, 1229–1240.e15. <https://doi.org/10.1016/j.cell.2016.10.046>.
49. Zhao, Y., Rai, J., and Li, H. (2023). Regulation of translation by ribosomal RNA pseudouridylation. *Sci. Adv.* 9, eadg8190. <https://doi.org/10.1126/sciadv.adg8190>.

50. Borovinskaya, M.A., Pai, R.D., Zhang, W., Schuwirth, B.S., Holton, J.M., Hirokawa, G., Kaji, H., Kaji, A., and Cate, J.H.D. (2007). Structural basis for aminoglycoside inhibition of bacterial ribosome recycling. *Nat. Struct. Mol. Biol.* *14*, 727–732. <https://doi.org/10.1038/nsmb1271>.
51. Prokhorova, I., Altman, R.B., Djumagulov, M., Shrestha, J.P., Urzhumtsev, A., Ferguson, A., Chang, C.-W.T., Yusupov, M., Blanchard, S.C., and Yusupova, G. (2017). Aminoglycoside interactions and impacts on the eukaryotic ribosome. *Proc. Natl. Acad. Sci. USA* *114*, E10899–E10908. <https://doi.org/10.1073/pnas.1715501114>.
52. Jansson, M.D., Häfner, S.J., Altinel, K., Tehler, D., Krogh, N., Jakobsen, E., Andersen, J.V., Andersen, K.L., Schoof, E.M., Ménard, P., et al. (2021). Regulation of translation by site-specific ribosomal RNA methylation. *Nat. Struct. Mol. Biol.* *28*, 889–899. <https://doi.org/10.1038/s41594-021-00669-4>.
53. Hirabayashi, N., Sato, N.S., and Suzuki, T. (2006). Conserved loop sequence of helix 69 in *Escherichia coli* 23 S rRNA is involved in A-site tRNA binding and translational fidelity. *J. Biol. Chem.* *281*, 17203–17211. <https://doi.org/10.1074/jbc.M511728200>.
54. Piel, L., Rajan, K.S., Bussotti, G., Varet, H., Legendre, R., Proux, C., Douché, T., Gial-Gianetto, Q., Chaze, T., Cokelaer, T., et al. (2022). Experimental evolution links post-transcriptional regulation to *Leishmania* fitness gain. *PLoS Pathog.* *18*, e1010375. <https://doi.org/10.1371/journal.ppat.1010375>.
55. Bussotti, G., Piel, L., Pescher, P., Domagalska, M.A., Rajan, K.S., Cohen-Chalamish, S., Doniger, T., Hiregange, D.-G., Myler, P.J., Unger, R., et al. (2021). Genome instability drives epistatic adaptation in the human pathogen *Leishmania*. *Proc. Natl. Acad. Sci. USA* *118*, e2113744118. <https://doi.org/10.1073/pnas.2113744118>.
56. McMahon, M., Contreras, A., Holm, M., Uechi, T., Forester, C.M., Pang, X., Jackson, C., Calvert, M.E., Chen, B., Quigley, D.A., et al. (2019). A single H/ACA small nucleolar RNA mediates tumor suppression downstream of oncogenic RAS. *Elife* *8*, e48847. <https://doi.org/10.7554/eLife.48847>.
57. Halfon, Y., Jimenez-Fernandez, A., La Rosa, R., Espinosa Portero, R., Krogh Johansen, H., Matzov, D., Eyal, Z., Bashan, A., Zimmerman, E., Belousoff, M., et al. (2019). Structure of *Pseudomonas aeruginosa* ribosomes from an aminoglycoside-resistant clinical isolate. *Proc. Natl. Acad. Sci. USA* *116*, 22275–22281. <https://doi.org/10.1073/pnas.1909831116>.
58. Muramatsu, T., Nishikawa, K., Nemoto, F., Kuchino, Y., Nishimura, S., Miyazawa, T., and Yokoyama, S. (1988). Codon and amino-acid specificities of a transfer RNA are both converted by a single post-transcriptional modification. *Nature* *336*, 179–181. <https://doi.org/10.1038/336179a0>.
59. Soma, A., Ikeuchi, Y., Kanemasa, S., Kobayashi, K., Ogasawara, N., Ote, T., Kato, J.i., Watanabe, K., Sekine, Y., and Suzuki, T. (2003). An RNA-Modifying Enzyme that Governs Both the Codon and Amino Acid Specificities of Isoleucine tRNA. *Mol. Cell* *12*, 689–698. [https://doi.org/10.1016/S1097-2765\(03\)00346-0](https://doi.org/10.1016/S1097-2765(03)00346-0).
60. Chothani, S., Adami, E., Ouyang, J.F., Viswanathan, S., Hubner, N., Cook, S.A., Schafer, S., and Rackham, O.J.L. (2019). deltaTE: Detection of Translationally Regulated Genes by Integrative Analysis of Ribo-seq and RNA-seq Data. *Curr. Protoc. Mol. Biol.* *129*, e108. <https://doi.org/10.1002/cpmb.108>.
61. Beneke, T., and Gluenz, E. (2019). LeishGEdit: A Method for Rapid Gene Knockout and Tagging Using CRISPR-Cas9. *Methods Mol. Biol.* *1971*, 189–210. [https://doi.org/10.1007/978-1-4939-9210-2\\_9](https://doi.org/10.1007/978-1-4939-9210-2_9).
62. Barth, S., Hury, A., Liang, X.H., and Michaeli, S. (2005). Elucidating the Role of H/ACA-like RNAs in trans -Splicing and rRNA Processing via RNA Interference Silencing of the *Trypanosoma brucei* CBF5 Pseudouridine Synthase. *J. Biol. Chem.* *280*, 34558–34568. <https://doi.org/10.1074/jbc.M503465200>.
63. Liang, X.-H., Uliel, S., Hury, A., Barth, S., Doniger, T., Unger, R., and Michaeli, S. (2005). A genome-wide analysis of C/D and H/ACA-like small nucleolar RNAs in *Trypanosoma brucei* reveals a trypanosome-specific pattern of rRNA modification. *RNA* *11*, 619–645. <https://doi.org/10.1261/ra.7174805>.
64. Li, H., Handsaker, B., Wysoker, A., Fennell, T., Ruan, J., Homer, N., Marth, G., Abecasis, G., and Durbin, R.; 1000 Genome Project Data Processing Subgroup (2009). The Sequence Alignment/Map format and SAMtools. *Bioinformatics* *25*, 2078–2079. <https://doi.org/10.1093/bioinformatics/btp352>.
65. Quinlan, A.R., and Hall, I.M. (2010). BEDTools: a flexible suite of utilities for comparing genomic features. *Bioinformatics* *26*, 841–842. <https://doi.org/10.1093/bioinformatics/btq033>.
66. Cox, J., and Mann, M. (2008). MaxQuant enables high peptide identification rates, individualized p.p.b.-range mass accuracies and proteome-wide protein quantification. *Nat. Biotechnol.* *26*, 1367–1372. <https://doi.org/10.1038/nbt.1511>.
67. Anders, S., Pyl, P.T., and Huber, W. (2015). HTSeq—a Python framework to work with high-throughput sequencing data. *Bioinformatics* *31*, 166–169. <https://doi.org/10.1093/bioinformatics/btu638>.
68. Dillon, L.A.L., Okrah, K., Hughitt, V.K., Suresh, R., Li, Y., Fernandes, M.C., Belew, A.T., Corrada Bravo, H., Mosser, D.M., and El-Sayed, N.M. (2015). Transcriptomic profiling of gene expression and RNA processing during *Leishmania major* differentiation. *Nucleic Acids Res.* *43*, 6799–6813. <https://doi.org/10.1093/nar/gkv656>.
69. Nguyen, A.M.T., Shalev-Benami, M., Rosa-Teijeiro, C., Ibarra-Meneses, A.V., Yonath, A., Bashan, A., Jaffe, C.L., Olivier, M., Fernandez-Prada, C., and Lubell, W.D. (2023). Systematic Exploration of Functional Group Relevance for Anti-*Leishmanial* Activity of Anisomycin. *Biomedicines* *11*, 2541. <https://doi.org/10.3390/biomedicines11092541>.
70. Zivanov, J., Nakane, T., Forsberg, B.O., Kimanius, D., Hagen, W.J., Lindahl, E., and Scheres, S.H. (2018). New tools for automated high-resolution cryo-EM structure determination in RELION-3. *Elife* *7*, e42166. <https://doi.org/10.7554/eLife.42166>.
71. Zheng, S.Q., Palovcak, E., Armache, J.-P., Verba, K.A., Cheng, Y., and Agard, D.A. (2017). MotionCorr2: anisotropic correction of beam-induced motion for improved cryo-electron microscopy. *Nat. Methods* *14*, 331–332. <https://doi.org/10.1038/nmeth.4193>.
72. Mindell, J.A., and Grigorieff, N. (2003). Accurate determination of local defocus and specimen tilt in electron microscopy. *J. Struct. Biol.* *142*, 334–347. [https://doi.org/10.1016/s1047-8477\(03\)00069-8](https://doi.org/10.1016/s1047-8477(03)00069-8).
73. Nakane, T., Kimanius, D., Lindahl, E., and Scheres, S.H. (2018). Characterisation of molecular motions in cryo-EM single-particle data by multi-body refinement in RELION. *Elife* *7*, e36861. <https://doi.org/10.7554/eLife.36861>.
74. Kucukelbir, A., Sigworth, F.J., and Tagare, H.D. (2014). Quantifying the local resolution of cryo-EM density maps. *Nat. Methods* *11*, 63–65. <https://doi.org/10.1038/nmeth.2727>.
75. Emsley, P., Lohkamp, B., Scott, W.G., and Cowtan, K. (2010). Features and development of Coot. *Acta Crystallogr. D Biol. Crystallogr.* *66*, 486–501. <https://doi.org/10.1107/S0907444910007493>.
76. Pettersen, E.F., Goddard, T.D., Huang, C.C., Meng, E.C., Couch, G.S., Croll, T.I., Morris, J.H., and Ferrin, T.E. (2021). UCSF ChimeraX: Structure visualization for researchers, educators, and developers. *Protein Sci.* *30*, 70–82. <https://doi.org/10.1002/pro.3943>.
77. Auffinger, P., Ennifar, E., and D’Ascenzo, L. (2020). Deflating the RNA Mg<sup>2+</sup> bubble. *Stereochemistry to the rescue!* *RNA* *27*, 243–252. <https://doi.org/10.1261/rna.076067.120>.
78. Rozov, A., Khusainov, I., El Omari, K., Duman, R., Mykhaylyk, V., Yusupov, M., Westhof, E., Wagner, A., and Yusupova, G. (2019). Importance of potassium ions for ribosome structure and function revealed by long-wavelength X-ray diffraction. *Nat. Commun.* *10*, 2519. <https://doi.org/10.1038/s41467-019-10409-4>.
79. Afonine, P.V., Poon, B.K., Read, R.J., Sobolev, O.V., Terwilliger, T.C., Urzhumtsev, A., and Adams, P.D. (2018). Real-space refinement in PHENIX for cryo-EM and crystallography. *Acta Crystallogr. D Struct. Biol.* *74*, 531–544. <https://doi.org/10.1107/S2059798318006551>.

80. Williams, C.J., Headd, J.J., Moriarty, N.W., Prisant, M.G., Videau, L.L., Deis, L.N., Verma, V., Keedy, D.A., Hintze, B.J., Chen, V.B., et al. (2018). MolProbity: More and better reference data for improved all-atom structure validation. *Protein Sci.* 27, 293–315. <https://doi.org/10.1002/pro.3330>.
81. Yamauchi, Y., Taoka, M., Nobe, Y., Izumikawa, K., Takahashi, N., Nakayama, H., and Isobe, T. (2013). Denaturing reversed phase liquid chromatographic separation of non-coding ribonucleic acids on macro-porous polystyrene-divinylbenzene resins. *J. Chromatogr. A* 1312, 87–92. <https://doi.org/10.1016/j.chroma.2013.09.021>.
82. Taoka, M., Nobe, Y., Hori, M., Takeuchi, A., Masaki, S., Yamauchi, Y., Nakayama, H., Takahashi, N., and Isobe, T. (2015). A mass spectrometry-based method for comprehensive quantitative determination of post-transcriptional RNA modifications: the complete chemical structure of *Schizosaccharomyces pombe* ribosomal RNAs. *Nucleic Acids Res.* 43, e115. <https://doi.org/10.1093/nar/gkv560>.
83. Nakayama, H., Yamauchi, Y., Taoka, M., and Isobe, T. (2015). Direct Identification of Human Cellular MicroRNAs by Nanoflow Liquid Chromatography–High-Resolution Tandem Mass Spectrometry and Database Searching. *Anal. Chem.* 87, 2884–2891. <https://doi.org/10.1021/ac504378s>.
84. Nakayama, H., Nobe, Y., Koike, M., and Taoka, M. (2023). Liquid Chromatography–Mass Spectrometry-Based Qualitative Profiling of mRNA Therapeutic Reagents Using Stable Isotope-Labeled Standards Followed by the Automatic Quantitation Software Ariadne. *Anal. Chem.* 95, 1366–1375. <https://doi.org/10.1021/acs.analchem.2c04323>.
85. Nakayama, H., Akiyama, M., Taoka, M., Yamauchi, Y., Nobe, Y., Ishikawa, H., Takahashi, N., and Isobe, T. (2009). Ariadne: a database search engine for identification and chemical analysis of RNA using tandem mass spectrometry data. *Nucleic Acids Res.* 37, e47. <https://doi.org/10.1093/nar/gkp099>.
86. Love, M.I., Huber, W., and Anders, S. (2014). Moderated estimation of fold change and dispersion for RNA-seq data with DESeq2. *Genome Biol.* 15, 550. <https://doi.org/10.1186/s13059-014-0550-8>.

## STAR★METHODS

### KEY RESOURCES TABLE

REAGENT or RESOURCE	SOURCE	IDENTIFIER
<b>Antibodies</b>		
mCherry primary antibody	Santa Cruz Biotechnology	Cat# SC-40
Secondary IgG antibody	Jackson	Cat# 115-035-062
<b>Chemicals, peptides, and recombinant proteins</b>		
Cyclohexamide	Sigma-Aldrich	Cat# C7698
Hydrazine monohydrate	Sigma-Aldrich	Cat# 207942
Aniline	Sigma-Aldrich	Cat# 242284
FastAP Thermosensitive Alkaline Phosphatase	Thermo Scientific	Cat# EF0651
Dynabeads® mRNA DIRECT™ Kit 40prep	Thermo Scientific	Cat# 6012
VAHTS DNA clean beads	Vasyme	Cat# N411-02
T4 RNA Ligase 1	New England Biolabs	Cat# M0437M
RNase Inhibitor Murin	New England Biolabs	Cat# M0314S
Dynabeads® MyOne™ SILANE beads	Invitrogen by Thermo Fisher Scientific	Cat# 37002D
AffinityScript Reverse Transcriptase enzyme	Agilent Technologies	Cat# 600107
NEBNext® High-Fidelity polymerase	New England Biolabs	Cat# M0541S
E-Gel EX agarose gel	Invitrogen by Thermo Fisher Scientific	Cat# G4010004
NucleoSpin Gel and PCR Clean-up kit	Macherey-Nagel GmbH & co.	Cat# 740609
NextSeq 500/550 High Output Kit v2.5 (75 Cycles)	Illumina	Cat# 20024906
Acetonitrile	FUJIFILM Wako Chemicals	Cat# 018-19853
Diammonium phosphate	FUJIFILM Wako Chemicals	Cat# 016-03325
Methanol	FUJIFILM Wako Chemicals	Cat# 134-14523
Triethylamine Acetate, pH = 7	Glen Research	Cat# 60-4110-60
<b>Critical commercial assays</b>		
Click-iT® AHA (L-azidohomoalanine) reagent (Invitrogen)	Invitrogen by Thermo Fisher Scientific	Cat# C10289
<b>Experimental models: Organisms/Strains</b>		
L. donovani strain 1S (MHOM/SD/62/1S-CL2D)	purified from the liver of infected hamsters	NA
L. major starin Friedlin V1 (MHOM/IL/80/Friedlin)	purified from the footpad of infected nude mice	NA
L. amazonensis strain LV79 (MPRO/BR/1972/M1841) expressing mcherry	purified from the footpad of infected nude mice	NA
Mesocricetus auratus (golden hamster)	JanvierLabs	Cat# HN-AU-59-F
NMRI-nude mice	JanvierLabs	Cat# SM-NU-5S-F
<b>Oligonucleotides</b>		
The complete list of oligonucleotides are presented in <a href="#">Table S12</a>	This study	NA
<b>Deposited data</b>		
Cryo-EM map and model of Parental strain classical-PRE-ribosome	This study	EMD-19576, PDB ID: 8RXH
Cryo-EM map and model of LM32CS3H1 sKO classical-PRE-ribosome	This study	EMD-19582, PDB ID: 8RXX
Cryo-EM map and model of Parental strain vacant 80S ribosome	This study	EMD-17216, PDB ID: 8OVJ

(Continued on next page)

<b>Continued</b>		
REAGENT or RESOURCE	SOURCE	IDENTIFIER
Cryo-EM map and model of LM32CS3H1 sKO vacant 80S ribosome	This study	EMD-15272, PDB ID: 8A98
RNA -sequencing data (NCBI BioProject database)	This study	PRJNA813383
Proteome (ProteomeXchange Consortium)	This study	PXD034116
<b>Software and algorithms</b>		
FASTX toolkit	Cold Spring Harbor Laboratory	<a href="http://hannonlab.csh.edu/fastx_toolkit">http://hannonlab.csh.edu/fastx_toolkit</a>
SMALT v0.7.5	Wellcome Sanger Institute	<a href="https://www.sanger.ac.uk/tool/smalt/">https://www.sanger.ac.uk/tool/smalt/</a>
Samtools v1.9	Genome Research Limited	<a href="https://www.htslib.org/">https://www.htslib.org/</a>
BEDtools v2.26.0 Suite	University of Utah	<a href="https://bedtools.readthedocs.io/en/latest/">https://bedtools.readthedocs.io/en/latest/</a>
HTSeq-count	European Molecular Biology Laboratory	<a href="https://htseq.readthedocs.io/en/release_0.11.1/count.html">https://htseq.readthedocs.io/en/release_0.11.1/count.html</a>
DTEG.R	Duke-NUS Medical School	<a href="https://github.com/SGDDNB/translational_regulation/blob/master/DTEG.R">https://github.com/SGDDNB/translational_regulation/blob/master/DTEG.R</a>
EMBOSS package (v6.6.0.0)	Sanger Center, Wellcome Trust Genome Campus	<a href="https://emboss.sourceforge.net/">https://emboss.sourceforge.net/</a>
Cordon (v1.6.0)	<a href="http://bioinfo.hr/">http://bioinfo.hr/</a>	<a href="https://github.com/BioinfoHR/coRdon">https://github.com/BioinfoHR/coRdon</a>
ggplot2 package	<a href="https://ggplot2.tidyverse.org/">https://ggplot2.tidyverse.org/</a>	<a href="https://github.com/tidyverse/ggplot2">https://github.com/tidyverse/ggplot2</a>
ImageJ	ImageJ	<a href="https://imagej.nih.gov/ij">https://imagej.nih.gov/ij</a>
RELION-4.0.1	MRC-LMB	<a href="https://www3.mrc-lmb.cam.ac.uk/relion/index.php/Main_Page">https://www3.mrc-lmb.cam.ac.uk/relion/index.php/Main_Page</a>
Phenix-1.20.1-4487	Afonine et al., 2018	<a href="https://phenix-online.org/">https://phenix-online.org/</a>
COOT	MRC-LMB	<a href="https://www2.mrc-lmb.cam.ac.uk/personal/pemsley/coot/">https://www2.mrc-lmb.cam.ac.uk/personal/pemsley/coot/</a>
UCSF ChimeraX	UCSF	<a href="https://www.cgl.ucsf.edu/chimera/">https://www.cgl.ucsf.edu/chimera/</a>
EMAN2	Baylor college of Medicine	<a href="https://blake.bcm.edu/emanwiki/EMAN2">https://blake.bcm.edu/emanwiki/EMAN2</a>
Ariadne	Riken	<a href="https://ariadne.riken.jp/">https://ariadne.riken.jp/</a>
<b>Others</b>		
Quantifoil R2/2 200 Mesh, copper, +2nm Carbon	Electron Microscopy Sciences	Cat# Q2100CR2-2NM

## RESOURCE AVAILABILITY

### Lead contact

Further information and requests for resources and reagents should be directed to and will be fulfilled by the lead contact, Shulamit Michaeli ([Shulamit.Michaeli@biu.ac.il](mailto:Shulamit.Michaeli@biu.ac.il)).

### Materials availability

The materials generated in this study are available from the [lead contact](#) upon request.

### Data and code availability

- All sequencing data related to this study have been deposited in the NCBI BioProject database under the accession number PRJNA813383. The mass spectrometry proteomics data have been deposited to the ProteomeXchange Consortium via the PRIDE partner repository with the dataset identifier PXD034116. The cryo-EM density maps of the *L. major* 80S ribosome have been deposited in the Electron Microscopy DataBank (EMDB) under accession numbers EMD-19576, EMD-19582, EMD-17216, and EMD-15272. Atomic coordinates and structure factors have been deposited in the Protein DataBank (PDB) under accession codes PDB: 8RXH, 8RXX, 8OVJ, and 8A98.
- Scripts used to analyze HydraPsiSeq and  $\Psi$ -seq are available at [https://github.com/michaelilab/LM\\_Psi\\_Paper](https://github.com/michaelilab/LM_Psi_Paper).
- Any additional information required to reanalyze the data reported in this paper is available from the [lead contact](#) upon request.

## EXPERIMENTAL MODEL AND STUDY PARTICIPANT DETAILS

### Animals and parasites

Female Golden Syrian hamsters (*Mesocricetus auratus* RjHan:AURA) weighing 60–70 g, six-week-old female and NMRI-nu mice were purchased from Janvier Laboratories (Le Genest-Saint-Isle, France), and handled under specific pathogen-free conditions in A3 animal facilities accredited by the French Ministry of Agriculture for performing experiments on live rodents (agreement A 75-15-01-2). Work on animals was performed in compliance with French and European regulations on care and protection of laboratory animals (EC Directive 2010/63, French Law 2013-118, February 6th, 2013). All experiments were approved by the Ethics Committee of the Institut Pasteur (C2EA n° 89) and the Ministère de l'enseignement supérieur, de la recherche et de l'innovation and registered under the reference #19683.

*L. donovani* strain Ld1S (MHOM/SD/62/1S-CL2D) was propagated in hamsters, *L. major* strain Friedlin FV1 (MHOM/IL/80/Friedlin) and *L. amazonensis* strain LV79 (MPRO/BR/1972/M1841) expressing mCherry were propagated in NMRI-nu mice. Amastigotes were purified from cutaneous lesions (LV79 and FV1) and livers (Ld1S) of infected animals.

*L. donovani* and *L. amazonensis* promastigotes were differentiated from animal-derived amastigotes and maintained in M199 complete medium (M199, 10% FBS, 25 mM HEPES; 100  $\mu$ M adenine, 2 mM L-glutamine, 10  $\mu$ g/mL folic acid, 13.7  $\mu$ M hemin, 4.2 mM NaHCO<sub>3</sub>, 1xRPMI1640 vitamins, 8  $\mu$ M 6-biopterin, 100 units penicillin and 100  $\mu$ g/mL streptomycin, pH 7.4. *L. major* promastigotes were also differentiated from animal-derived amastigotes and maintained in M199, 10% FBS, 25 mM HEPES; 100  $\mu$ M adenine, 2 mM L-glutamine, biotin 1  $\mu$ g/mL, 13.7  $\mu$ M hemin, 4.2 mM NaHCO<sub>3</sub>, 100 units penicillin and 100  $\mu$ g/mL streptomycin, pH 7.4.

## METHOD DETAILS

### Generation of transgenic *L. major* parasites

To generate *L. major* (Friedlin strain) overexpressing LM32Cs3H1 snoRNA, the regions flanking the snoRNA was cloned into pX-Neo plasmid<sup>36</sup> using the primers listed in Table S9. Site-directed mutagenesis was performed to introduce mutations in the pseudouridylation pocket. The template plasmid was digested with *DpnI* (NEB), and clones were isolated. *L. major* promastigotes expressing mCherry-MYC were generated by transfecting an episomal pPLOTv1-Neo-mCherry-Neo plasmid (a gift from Dr. Eva Gluenz, Institute of Cell Biology, University of Bern, Switzerland) and selection with G418. For the expression of spCas9 and T7 polymerase in *L. major*, an episomal pTB007 plasmid was transfected and selected using hygromycin.<sup>61</sup> snoRNA-specific guide RNAs (gRNAs) were designed using the EuPaGDT database (<http://grna.ctegd.uga.edu/>) and *in vitro* transcribed. To prepare homologous DNA repair (HDR) templates, PLOTv1-PURO plasmid, which carries puromycin resistance, was used as a template for PCR amplification. The primers used for gRNA synthesis and HDR template are listed in Table S9. Both gRNAs and the snoRNA-specific PCR product were transfected, selected using antibiotics, single cells were cloned using Fluorescence-activated cell sorting (FACS), and knockout cells were screened by Northern analysis and PCR (57).

### Monitoring amastigote parasites within infected macrophages

THP1 monocytes were cultured in RPMI supplemented with L-glutamine (5%) and 10% FCS. Maturation of the THP1 cells into macrophages was induced by addition of 50 ng/mL of Phorbol 12-Myristate 13-Acetate for 48 h in 12 well plates containing round sterile coverslip. Upon incubation for 48 h, the culture medium was removed and replaced by fresh medium. Stationary phase *L. major* promastigotes tagged with mCherry were added to the cells at a ratio of 1:6 (macrophage:parasite). After 24 h post infection, two washes with 1X PBS were performed to remove free parasites, and the nuclei were stained with NucBlue Live reagent/Hoechst 33342 dye (Thermo Scientific). Live images were acquired with a Leica SP8 confocal microscope using a  $\times$ 100 HC Plan-Apo 1.4 NA objective at 512  $\times$  512 pixels with Z slices taken every 200 nm. The images were then deconvolved using Huygens Professional software with standard parameters (SVI, Laapersveld 6, 1213 VB Hilversum, The Netherlands). The number of parasites expressing mCherry and the total number of infected cells were counted manually using ImageJ software (<https://imagej.nih.gov/ij/>). More than 50 cells were counted in each field of view. At least eight images were collected for each condition.

### Preparation of H/ACA snoRNome

snoRNAs associated with the NHP2 (an H/ACA snoRNP) were isolated by the tandem affinity purification (TAP) method.<sup>34</sup> Accordingly, *L. donovani* cells ( $2 \times 10^{11}$  cells) overexpressing NHP2-TAP was washed twice with PBS and once with buffer-I (20 mM Tris-HCl (pH 7.7), 150 mM KCl, and 3 mM MgCl<sub>2</sub>). The cells were resuspended in 15 mL of buffer-II (buffer-I with 1 mM DTT and 10  $\mu$ g/mL leupeptin), equilibrated by nitrogen cavitation (Parr Instruments Co.) at 750 p.s.i. N<sub>2</sub> for 1 h at 4°C, and disrupted by release. After release of the pressure, protease inhibitor mixture (Roche Applied Science) was added, and the extract was treated with 0.5% Triton X-100. The extract was incubated at 4°C for 15 min, passed through a syringe, cleared of cell debris by centrifugation (15,000  $\times$ g), and the supernatant was incubated with rabbit IgG-agarose beads (200  $\mu$ L) (Sigma) while rotating for 2 h. The beads were washed 5 times with TEV-buffer (buffer-I with 0.5 mM DTT, 0.5 mM EDTA) and incubated overnight in 1.5 mL of TEV-buffer with 200 units of tobacco etch virus protease (Promega). After centrifugation, the supernatant was incubated with 50  $\mu$ L of Strep-T actin-Sepharose beads (IBA) for 1 hr. The beads were washed with buffer-III (TEV-buffer with 2 mM CHAPS (GE Healthcare)), and the complexes were

eluted with elution buffer (100 mM Tris-Cl (pH 8), 150 mM NaCl, 1 mM EDTA) containing 2.5 mM d-desthiobiotin (Sigma). The RNA associated with NHP2 was recovered by phenol: chloroform extraction, and ethanol precipitation.

RNA extracted from the elution was used for library preparation, essentially as described. Briefly, 800ng of RNA was dephosphorylated with FastAP Thermosensitive Alkaline Phosphatase (Thermo Scientific), cleaned by Agencourt RNA clean XP beads (Beckman Coulter) and ligated to 3' linker using high concentration T4 RNA Ligase 1 (NEB) in a buffer containing DMSO, ATP, PEG 8000 and RNase inhibitor (NEB). The ligated RNA was cleaned from excess linker using Dynabeads MyOne SILANE beads (Thermo Scientific), and first strand cDNA was prepared using the AffinityScript Reverse Transcriptase enzyme (Agilent). The RNA was subsequently degraded using 2 $\mu$ L of 1M NaOH and the cDNA was cleaned using Dynabeads MyOne SILANE beads (Thermo Scientific). The cDNA was further ligated to the 3' adapter using high concentration T4 RNA Ligase 1 (NEB) and cleaned of excess adapter by using Dynabeads MyOne SILANE beads (Thermo Scientific). The adapter ligated cDNA was PCR enriched using NEBNext High-Fidelity (NEB) polymerase (9 PCR cycles), separated on an E-Gel EX agarose gel (Invitrogen) and size selected at the range of 150–300 bp (containing ~30–180nt corresponding to RNA). The amplicons were gel purified using NucleoSpin Gel and PCR Clean-up kit (Macherey-Nagel) and sequenced in a Nextseq system (Illumina) in paired end mode (40 million reads for each sample). The L. major NHP2 tandem affinity purification data were derived from our previous study.<sup>34</sup>

### Northern analysis

For Northern analysis, total RNA was extracted and separated on a 10% acrylamide denaturing gel. Antisense RNA probes were prepared by *in-vitro* transcription using  $\alpha$ -<sup>32</sup>P-UTP.<sup>62,63</sup> Primers used for *in-vitro* transcription are listed in Table S9.

### (N-cyclohexyl-N'- $\beta$ -(4-methylmorpholinium) ethylcarbodiimide *p*-tosylate) treatment

RNA was treated with (N-cyclohexyl-N'- $\beta$ -(4-methylmorpholinium) ethylcarbodiimide *p*-tosylate) (CMC) in bicine buffer (0.17 M CMC in 50 mM bicine, pH 8.3, 4 mM EDTA, 7 M urea) at 37°C for 20 min. Excess CMC was removed by ethanol precipitation. To remove CMC groups attached to G and U, the CMC-treated RNA was subjected to alkali hydrolysis with Na<sub>2</sub>CO<sub>3</sub> (50 mM, pH 10. 4) at 37°C for 4h, as previously described.<sup>14–16</sup> The reacted RNA was recovered by phenol: chloroform extraction, and ethanol precipitation.

### $\Psi$ -seq and detection of pseudouridylated sites

To perform  $\Psi$ -seq, an adaptor was ligated to the 3' end of the total RNA (upon fragmentation) before and after CMC treatment, and cDNA was prepared using AffinityScript reverse transcriptase (Agilent). The cDNA was then ligated to an adaptor, PCR amplified, and the samples were sequenced in an Illumina NextSeq machine in paired end mode (20 million reads for each sample).

The 42 bp sequence reads obtained from the Illumina Genome Analyzer were first trimmed of Illumina adapters using the FASTX toolkit ([http://hannonlab.cshl.edu/fastx\\_toolkit](http://hannonlab.cshl.edu/fastx_toolkit)), and reads of 15 bases or less were discarded from subsequent analysis. The remaining reads were mapped to the *Leishmania* genome using SMALT v0.7.5 (<http://www.sanger.ac.uk/resources/software/smalt/>) with the default parameters. The *Leishmania* genomes used in this study are Sudanese L. *donovani* strain 1S2D (Ld1S) (<https://www.ncbi.nlm.nih.gov/bioproject/PRJNA396645>), TriTrypDB-47\_Lamazonensis MHOMBR71973M2269\_Genome (<https://tritrypdb.org/tritrypdb/app/downloads/release-47/LamazonensisMHOMBR71973M2269/fasta/data/>), TriTrypDB9.0\_LmajorFriedlin\_Genome (<https://tritrypdb.org/tritrypdb/app/downloads/release-9.0/LmajorFriedlin/fasta/data/>). The rRNA sequence used in this study are available in [https://github.com/michaelilab/LM\\_Psi\\_Paper/tree/main/DB](https://github.com/michaelilab/LM_Psi_Paper/tree/main/DB). Only properly paired partners were retained. Each read pair was “virtually” extended to cover the area from the beginning of the first read to the end of its partner. For each base, the number of reads initializing at that location as well as the number of reads covering the position were calculated. A combination of Bedtools (<http://bedtools.readthedocs.io/en/latest/>) and in-house Perl scripts was used to calculate the  $\Psi$ -ratio and  $\Psi$ -fc (fold change), as previously described. For each nucleotide, we computed the  $\Psi$ -ratio, dividing the number of reads covering that nucleotide by the number of nucleotides initiating at the following base (i.e., corresponding to the last position copied by the reverse transcriptase). This was performed for both (-CMC) and (+CMC) samples. The  $\Psi$ -fc(log<sub>2</sub>) was computed as the log<sub>2</sub>-fold change of the  $\Psi$ -ratios in (-CMC) versus the (+CMC).<sup>14–16</sup>

### Hydrazine and aniline treatment

Total RNA and polysomal RNA (5 $\mu$ g) were treated with 50% hydrazine (Sigma) for 45 min on ice, and ethanol precipitated.<sup>35</sup> The RNA pellet was then resuspended in 1M aniline (Sigma) (pH 4.5 adjusted using glacial acetic acid) until the white pellet was completely dissolved, boiled for 15 min at 60°C in the dark, and immediately placed on ice. The fragmented RNA was recovered by ethanol precipitation and used for library preparation.<sup>14,16</sup>

### HydraPsiSeq library preparation

To perform HydraPsiSeq, the fragmented RNA (~800ng) was dephosphorylated with FastAP Thermosensitive Alkaline Phosphatase (Thermo Scientific), cleaned by Agencourt RNA clean XP beads (Beckman Coulter) and ligated to a 3' linker using high concentration T4 RNA Ligase 1 (NEB) in a buffer containing DMSO, ATP, PEG 8000, and RNase inhibitor (NEB). The ligated RNA was cleaned from excess linker using Dynabeads MyOne SILANE beads (Thermo Scientific), and first strand cDNA was prepared using the AffinityScript Reverse Transcriptase enzyme (Agilent). The RNA was subsequently degraded using 2 $\mu$ L of 1 M NaOH, and the cDNA was cleaned using Dynabeads MyOne SILANE beads (Thermo Scientific). The cDNA was further ligated to a 3' adapter using

T4 RNA Ligase 1 (NEB) at high concentration and cleaned of excess adapter by using Dynabeads MyOne SILANE beads (Thermo Scientific). The adapter-ligated cDNA was PCR enriched using NEBNext High-Fidelity (NEB) polymerase (9 PCR cycles), separated on an E-Gel EX agarose gel (Invitrogen), and size selected at the range of 150–300 bp (containing ~30–180 nt corresponding to RNA). The amplicons were gel purified using NucleoSpin Gel and PCR Clean-up kit (Macherey-Nagel) and sequenced in a Nextseq system (Illumina) in paired end mode (20 million reads for each sample).

### HydraPsiSeq data analysis

The paired end reads obtained from each sample were aligned to the *Leishmania* genome using SMALT v\_0.7.5 (<http://www.sanger.ac.uk/resources/software/SMALT/>) with default parameters. For each sample, the resulting bam file was sorted and filtered for proper pairs using Samtools v1.9<sup>64</sup> and then converted to a BED file using the bamtoBED module from the BEDtools v2.26.0 Suite.<sup>65</sup> Using an in-house Perl script on each bed file, the number of reads whose 5'-end alignments initiate at that base for each position on the rRNA was calculated. The total coverage for each base was calculated using the genomcov module from the BEDtools v2.26.0 Suite.<sup>65</sup> These files were then used as input for the R scripts (<https://github.com/FlorianPichot/HydraPsiSeqPipeline>), as previously described.<sup>35</sup>

### Proteolysis and dimethyl labeling

Cells lysed using RIPA (Sigma) buffer were precipitated in 80% ethanol, and the protein pellets were dissolved in (8.5M Urea, 10mM DTT, 400 mM ammonium bicarbonate (ABC)), sonicated twice (90%, 10-10 cycles, 5'), and centrifuged. The proteins in the solution were reduced (60°C for 30 min), modified with 35.2mM iodoacetamide in 100mM ammonium bicarbonate (in the dark, at room temperature for 30 min) and digested in 1.5M Urea, 70mM ABC with modified trypsin (Promega) at a 1:50 enzyme-to-substrate ratio, overnight at 37°C. A second digestion was done with modified trypsin at a concentration of 1:100 (enzyme to substrate) for 4 h at 37°C. The resulting peptides were desalted using C18 Top tip columns (Glygen) dried and re-suspended in 50mM HEPES (pH 7.9). Labeling by dimethylation was done in the presence of 100mM NaCBH<sub>3</sub> (Sterogene, 1M), by adding Light Formaldehyde (35% Frutarom, 12.3M) to one of the samples, and Heavy Formaldehyde (20% w/w, Cambridge Isotope laboratories, 6.5M) to the other sample to a final concentration of 200mM. The samples were incubated for 1 h samples were neutralized with 1M ABC for 30min, and equal amounts of the light and heavy peptides (determined using Bradford assay) were mixed, cleaned on C18 Top tip columns, and re-suspended in 0.1% formic acid.

### Mass spectrometry analysis of proteins

The peptides were resolved by reverse-phase chromatography on 0.075 X 180-mm fused silica capillaries (J&W) packed with Re-prosil reversed phase material (Dr Maisch GmbH, Germany). The peptides were eluted with a linear 180 min gradient of 5–28%, a 15 min gradient of 28–95%, and 25 min at 95% acetonitrile with 0.1% formic acid in water, at a flow rate of 0.15 μL/min. Mass spectrometry was performed by Q-Exactive HFX mass spectrometer (Thermo Scientific) in positive mode using repetitively full MS scan followed by collision to induce dissociation (HCD) of the 30 most dominant ions selected from the first MS scan. The mass spectrometry data were analyzed using the Proteome Discoverer 1.4 (Thermo Scientific) software, searching against the *L. major* from the TriTrypDB v.35 database (<https://tritrypdb.org>). Results were filtered with rank 1 peptides and 1% false discovery rate. The ratios were normalized according to the protein's median ratio. Perseus software (<https://maxquant.net/perseus/>) was used for statistical analysis of the data. Significant outliers relative to a certain population were calculated using intensity-dependent calculation. The truncation was based on the Benjamini-Hochberg correction for multiple hypothesis testing (SignificanceB).<sup>66</sup> For combined analysis of different replicates, a one-sample t test was used to determine if the mean is significantly different from a fixed value (0). All MS analyses were performed at the Smoler Proteomics Center, Technion, Israel, and raw data are available via ProteomeXchange, with identifier PXD034116. The identity of heavy and light isotope labeled samples is listed in Extended Table S10.

### Methionine incorporation assay

*L. major* cells ( $5 \times 10^7$ ) were washed in methionine-free (phenol red free) SDM-79 media, treated with 50 μM Click-iT AHA (L-azidohomoalanine) reagent (Invitrogen) in methionine-free (phenol red free) SDM-79 media, and were incubated for 30 min at 27°C according to the manufacturer's protocol. The cells were fixed using 1.6% formaldehyde, and permeabilized with Triton:Tween 20 (1:0.1%) in 1xPBS. The cells were incubated with Click-iT reaction cocktail for 30 min and washed once with 3% BSA in 1xPBS. The incorporated Click-iT AHA was determined by FACS Aria using the Alexa 488 channel.

### Translation efficiency and mRNA characteristics analysis

Poly (A) RNA sequencing reads were aligned to the *L. major* Friedlin (v9) genome using SMALT (v0.7.5). Raw read counts were quantified using HTSeq-count.<sup>67</sup> Differential translation efficiency (TE) was calculated using poly (A) RNA derived from polysomes and total cell lysate, using DTEG.R.<sup>60</sup> The GC-content of the differentially translated genes was computed using the "geecee" program from the EMBOSS package (v6.6.0.0). UTR lengths for *L. major* mRNAs were calculated based on the dominant 5' SL sites and 3' poly (A) sites.<sup>68</sup> Codon usage analysis was determined using the R package, Cordon (v1.6.0) (.com/BioinfoHR/coRdon). Briefly, the software calculates the Synonymous Codon Usage Order (SCUO), the codon usage bias in a set of coding sequences by assigning a codon usage order score to each synonymous codon. The codon usage order score represents the frequency of each codon in

a sequence compared to the expected frequency based on the overall codon usage bias in the sequence. Significant differences between differentially translated mRNA species were determined using the Wilcoxon test. The volcano plots, boxplots and other plots were created in R (v4.2.2) using the ggplot2 package (<https://github.com/tidyverse/ggplot2>).

### Fractionation of ribosomes on sucrose gradient

Whole cell extracts were prepared from  $5 \times 10^9$  *L. major* cells in a buffer containing 150mM KCL, 20mM Tris-pH 7.6, 10mM MgCl<sub>2</sub>, 0.5M DTT and 0.1% NP-40. In addition, 1  $\mu$ L leupeptin (10 mg/ml) protease inhibitor, and 1  $\mu$ L of Rnasin (Thermo Scientific) were added to the lysate. Cells were lysed using nitrogen cavitation (90 bar, 45 min, 4°C) and cell debris was removed by centrifugation (30 min at 8000 rpm) at 4°C. Lysate (400 $\mu$ L) were fractionated on a 10–30% or 15–50% (w/v) sucrose gradient by centrifugation at 35,000 rpm for 3 h or 70,000 rpm for 1.5 h respectively in a Beckman SW41 rotor at 4°C. The fraction carrying ribosomes was ethanol precipitated, and ribosomes were resuspended in buffer-150 (150mM KCL, 20mM Tris-pH 7.6, 10mM MgCl<sub>2</sub>) and used for mass spectrometry analysis. For preparation of polysome fractions, the cells were incubated with 50  $\mu$ g/ml cycloheximide for 15 min prior to cell lysis and 100  $\mu$ g/ml cycloheximide was added to all buffers mentioned above. tRNAs bound to translating ribosomes were released by incubating polysome fraction in ribosome-splitting buffer (20 mM Tris-pH 7.5, 300 mM KCl, 2 mM MgCl<sub>2</sub>, 1 mM DTT and 2 mM puromycin). The disassociated ribosome subunits (60S and 40S) were centrifuged at 55,000 rpm at 4°C for 15 h (Ti70 rotor, Beckman) and the supernatant was used for RNA isolation using standard Trizol/chloroform method. tRNAs were deacetylated in 0.5M Tris-HCL pH 9 for 4 h in 25°C, RNA was recovered by ethanol precipitation and 800 ng RNA was used for library preparation.

### Purification of 80S ribosomes for cryo-EM

Mid-log phase *L. major* cells ( $1.5\text{--}2 \times 10^7$  cells/ml,  $\sim 1$ g pellet) were washed three times in resuspension buffer (45 mM HEPES-KOH pH 7.6, 100 mM KOAc, 10 mM Mg(OAc)<sub>2</sub> and 250 mM Sucrose) and then suspended in cold buffer-A (45 mM HEPES-KOH pH 7.6, 100 mM K(OAc), 10 mM Mg(OAc)<sub>2</sub>, 250 mM Sucrose, 5 mM  $\beta$ -mercaptoethanol and a 1:40 dilution of Rnasin U (Promega). Cells were lysed using nitrogen cavitation (750 p.s.i. N<sub>2</sub>, 45 min, 4°C) and cell debris, was removed by centrifugation (30 min at 9000 rpm) at 4°C. The lysate was gently loaded onto a 1.1 M sucrose cushion in cold buffer-B (20 mM HEPES-KOH pH 7.6, 150 mM KOAc, 10 mM Mg(OAc)<sub>2</sub>, 1.1 M sucrose and 5 mM  $\beta$ -mercaptoethanol) and centrifuged at 55,000 rpm at 4°C for 15 h (Ti70 rotor, Beckman). Upon centrifugation, the pellet was resuspended in cold buffer-C (20 mM HEPES-KOH pH 7.6, 150 mM KOAc, 10 mM Mg(OAc)<sub>2</sub> and 5 mM  $\beta$ -mercaptoethanol) and loaded onto to a 10–40% (w/v) sucrose gradient in buffer-C for centrifugation (22,000 rpm, 11 h, on SW28 rotor, Beckman). The peak corresponding to 80S ribosomes was collected, balanced with buffer-C and centrifuged at 55,000 rpm for 12 h at 4°C. The resulting pellet was suspended in buffer-D (20 mM HEPES-KOH pH 7.6, 100 mM KOAc, 10 mM Mg(OAc)<sub>2</sub>, 10 mM NH<sub>4</sub>OAc and 1 mM DTT) and centrifuged for 90 min at 75,000 rpm (TLA-100 rotor, Beckman). The final ribosome pellet was gently resuspended in buffer-D, aliquots were flash frozen and stored in  $-80^\circ\text{C}$  until further use. The identity of 80S was further confirmed by mass spectrometry analysis.

### Ternary 80S complex formation with mRNA and tRNAs

To reconstitute the classical-PRE-ribosome complex with mRNA and three tRNA molecules we sequential mixed vacant 80S ribosomes with mRNA fragment coding for MET (AUG) and PHE (UUC) codons (CACCAUGUUC<sub>3</sub>AAA, Integrated DNA Technologies, Inc.), a P-site tRNA<sup>fMet</sup> (*E. coli*, Sigma) and an A-site tRNA<sup>Phe</sup> (*E. coli*, Sigma) at a 1:100:5:5 stoichiometric ratio. To restrict the peptidyl-transferase center, an anisomycin analog was used at 100 $\mu$ M concentration.<sup>69</sup> The complex assembly was performed at 37 °C in buffer-D (20 mM HEPES-KOH pH 7.6, 100 mM KOAc, 10 mM Mg(OAc)<sub>2</sub>, 10 mM NH<sub>4</sub>OAc and 1 mM DTT) with relaxation time of 15 min after addition of each component.

### Cryo-EM data collection and refinement

To prepare cryo-EM grids, 3.5  $\mu$ L of ribosome suspension ( $\sim 10$ A of A<sub>260</sub>) was applied onto glow-discharged holey carbon grids (Quantifoil R2/2) coated with a continuous thin carbon film. The grids were blotted and plunge-frozen using Vitrobot Mark IV (Thermo Fischer Scientific). A Titan Krios electron microscope (Thermo Fischer Scientific) operating at 300 kV equipped with K3 direct electron detector (Gatan Inc.) was used for collecting cryo-EM micrographs at liquid nitrogen temperature at a nominal magnification of X105,000, with a pixel size of 0.85 Å/pixel and a dose rate of  $\sim 1$  electron/Å<sup>2</sup>/frame. Defocus values ranged from  $-0.5$  to  $-1.5$   $\mu$ m. Relion 3.1 was used for data processing.<sup>70</sup> Motion correction and contrast transfer function parameters were estimated using Motioncor2<sup>71</sup> and CTFIND-3,<sup>72</sup> respectively. The extracted particles were subjected to several rounds of unsupervised 3D classification using a low-pass filtered cryo-EM density map. 3D classes similar to 80S particles were selected and subjected to auto-refinement in Relion 3.1. Upon initial refinement, particles were subjected to CTF refinement, Bayesian polishing, and refinement. The resulting high-resolution 3D density map was then subjected to a cycle of multibody refinement using separate masks for the large subunit (LSU), the head, and body regions of SSU.<sup>73</sup> The gold standard Fourier shell correlation (FSC) value criterion of 0.143 was used for determining averaged map resolutions, as implemented in Relion 3.1. Local resolution was estimated using Resmap.<sup>74</sup>

### Model building and refinement

rRNA and ribosomal protein models were built by template-guided model building in COOT.<sup>75</sup> The coordinates of the *L. donovani* ribosome (PDB ID: 5T2A, 6AZ1 and 6AZ3) were used as a template for model building and were docked onto density maps using UCSF ChimeraX.<sup>76</sup> RNA modifications were manually modeled based on  $\Psi$ -seq and HydraPsiSeq, as well as *L. donovani* cryo-EM and mass spectrometry information. The  $Mg^{2+}$ ,  $Zn^{2+}$ ,  $Na^+$ , and  $K^+$  ion compositions were modeled according to the recently described criteria.<sup>77,78</sup> Model refinement was performed using an iterative approach, including real-space refinement and geometry regularization in COOT,<sup>75</sup> followed by real-space refinement using the PHENIX suite.<sup>79</sup> The final model was validated using MolProbity.<sup>80</sup>

### Purification of rRNA subunits

*L. major* rRNAs were purified by using reversed-phase LC through a PLRP-S 4000Å column (4.6 × 150 mm, 8 μm, Agilent Technologies) from the total RNA. The rRNAs were eluted with a 120-min gradient of 10.8–13.6% (10.8–12.4% for the first 20 min and 12.4–13.6% for the next 100 min) (v/v) acetonitrile in 100 mM TEAA (pH 7.0) and 0.1 mM diammonium phosphate from the column at a flow rate of 200 μL/min at 60°C while monitoring the eluate at A260.<sup>81</sup>

### LC-MS and MS/MS analysis and database search of RNA fragments

Purified rRNA was digested with RNase T1, and the resulting RNA fragments were cyanoethylated for labeling pseudouridine.<sup>82</sup> The RNA fragments were analyzed with a direct nanoflow LC-MS system as described.<sup>83</sup> The column was prepared with a fused-silica capillary (150-μm i.d. × 240 mm in length) packed with a reversed-phase material (Develosil C30-UG-3, 3-μm particle size; Nomura Chemical). The LC was performed at a flow rate of 200 nL/min using a 120-min linear gradient from 10% to 7.6% methanol/9.8% acetonitrile in 10 mM triethylammonium acetate (pH 7.0). The eluate was sprayed online at –1.3 kV with the aid of a spray-assisting device to a Q Exactive Plus mass spectrometer (Thermo Fisher Scientific) in negative ion mode.<sup>84</sup> Ariadne<sup>85</sup> was used for database searches and assignment of MS/MS RNA spectra. The composite of *L. major* rRNA sequences was used as a database. The following default search parameters for Ariadne were used: maximum number of missed cleavages, 1; variable modification parameters, two modifications including cyanoethylation for uridine and methylation for any residue per RNA fragment; RNA mass tolerance, ±5 ppm, and MS/MS tolerance, ±20 ppm.

### Cell-free transcription-translation assay

To prepare *L. major* S12 lysates, equal number of mid-log phase PS and LM32CS3H1 sKO cells were washed three times and re-suspended in buffer-B containing Tris-acetate (10 mM), 60 mM KOAc, DTT (1 mM) and 14 mM Mg(OAc)<sub>2</sub> (12.7mL buffer-B for 10g cell pellet). Cells were lysed using nitrogen cavitation (750 p.s.i. N<sub>2</sub>, 45 min, 4°C) and cell debris was removed by centrifugation (30 min at 9000 rpm) at 4°C. The resulting S12 lysate was aliquoted and flash frozen in liquid nitrogen. To inhibit translation of endogenous mRNA, an anti-SL RNA oligonucleotide (5'-CAATAAAGTACAGAACTGATACTTATATAGCGTT-3') was used at 15 μM concentration. To monitor the translation activity of S12 lysates, GFP mRNA was transcribed from pLEXSY-*invitro2*-EGFP plasmid (Jena Bioscience) using T7 polymerase (Promega) in a mixture containing 260 μM amino acid mix, 600 μg/ml creatine-kinase, 300 μM spermidine, 10 μM Mg(OAc)<sub>2</sub>, 1 mM rNTP mix and LMCPY mix (HEPES-KOH, PEG 8000, Ammonium Acetate, Folinic acid, Tyrosine, Creatine Phosphate, Potassium Glutamate, DTT, cAMP-Na, Yeast tRNA mix). Translation assays were performed in black polystyrene 384-well flat-bottom plates (Greiner) at 37°C for 2hr. The fluorescence of GFP ( $\lambda$ (ex) = 488 nm;  $\lambda$ (em) = 507 nm) was measured using Tecan Infinite RF200 microplate reader (Tecan Group Ltd.). Heat-inactivated reaction mixture was used as negative control to monitor background fluorescence.

### QUANTIFICATION AND STATISTICAL ANALYSIS

All experiments were repeated three or more times unless indicated. Tandem LC-MS for rRNA modification was done only once. Statistical analysis and bar-graphs were prepared using Microsoft excel, Origin (OriginLab Corporation) and DESeq2 (v1.38.3).<sup>86</sup> ImageJ (<https://imagej.nih.gov/ij>) software was used for the analysis of western and northern blots. Canvas X (Canvas GFX, Inc.) was used for image arrangement and preparation of Figures.